BACHELOR THESIS

The effect of large amplitude internal wave (LAIW) and monsoon exposure on growth and skeletal density of the coral *Porites lutea*

Der Effekt von internen Wellen mit großer Amplitude (LAIW) und Monsun auf das Wachstum und die Skelettdichte der Koralle *Porites lutea*

submitted by

Kristina Kira Beck

Bremen, 10th of August 2015

Bentho-Pelagic Processes, Alfred Wegener Institute for Polar and Marine Research

Faculty of Biology/Chemistry, University of Bremen

First Examiner:	Prof. Dr. Claudio Richter Alfred Wegener Institute for Polar and Marine Research, Bremerhaven
Second Examiner:	Dr. Gernot Nehrke Alfred Wegener Institute for Polar and Marine Research, Bremerhaven
Supervisor:	Dr. Gertraud Schmidt Alfred Wegener Institute for Polar and Marine Research, Bremerhaven
	Dr. Marlene Wall GEOMAR – Helmholtz Centre for Ocean Research, Kiel

Universität Bremen*

ALFRED-WEGENER-INSTITUT
HELMHOLTZ-ZENTRUM FÜR POLAR- UND MEERESFORSCHUNG

Acknowledgements

Vielen Dank, Prof. Dr. Claudio Richter, dass du mir die Möglichkeit gegeben hast meine Bachelorarbeit über dieses interessante Thema zu schreiben.

Ein riesengroßer Dank geht an Dr. Gertraud Schmidt, für deine super Betreuung und Unterstützung bei meiner Bachelorarbeit sowie dein unglaubliches Engagement! Danke auch, dass du immer ein offenes Ohr für meine zahlreichen Fragen hattest und vielen Dank für deine Hilfe bei der statistischen Auswertung.

Ich danke auch Dr. Marlene Wall, für deine Betreuung und insbesondere für deine Hilfe bei der Auswahl und Durchführung der Methoden.

Ich möchte mich auch bei Dr. Gernot Nehrke dafür bedanken, dass du dich dazu bereiterklärt hast meine Bachelorarbeit zu begutachten.

Ulrike Holtz, vielen herzlichen Dank, dass du mich im Labor unterstützt und mir dort bei allen Problemen geholfen hast.

Vielen Dank an alle aus der Sektion Bentho-Pelagische Prozesse: dafür, dass ich mich bei Fragen immer an jemanden von euch wenden konnte und für eure Gesellschaft in den Mittagspausen. Insbesondere möchte ich mich bei Ulla Liebert dafür bedanken, dass du mir geholfen hast mich schnell am AWI und in der Sektion zurechtzufinden.

Bedanken möchte ich mich auch bei Constanze von Waldthausen, Kerstin Beyer und Michael Seebeck dafür, dass ich die Geräte in euren Laboren für meine Arbeit benutzen durfte und ihr mir bei der Durchführung meiner praktischen Arbeiten geholfen habt.

Ein ganz besonderer Dank geht auch an meine Familie und Freunde, für eure Unterstützung und Hilfe während der ganzen letzten drei Jahre und insbesondere in den letzten Monaten.

Contents

Abstract

The Similan Islands, a chain of islands in the Andaman Sea, are subject to large amplitude internal waves (LAIW, or solitons) and the southwest monsoon. The ocean facing west side of this archipelago near the Thai continental shelf break is exposed to LAIW and monsoon, whereas the eastern side is sheltered from both. LAIW mainly influence greater depth and are known to change environmental factors that affect coral growth. The monsoon however, causes higher wave action and increased sedimentation and therefore primarily influences shallow reef areas.

In the present study, the impact of LAIW and monsoon on linear extension rate, skeletal bulk density and calcification rate of the scleractinian coral *Porites lutea* are investigated. Coral skeletons have been collected at two depths (7 and 20 m) at the west and east sides of the central Similan island Ko Miang. X-radiography and fluorescence analysis are used to examine the linear extension rate due to the annual banding in the coral skeletons. Measurements of skeletal bulk density, micro-density and porosity are based on the buoyant weighing technique, calculation of the total enclosed volume and measurement of matrix volume by Archimedean methods.

Higher skeletal bulk densities were found at the west side of the island Ko Miang with highest values at W 7 m. As no correlation of the skeletal bulk density with the intensity of LAIW was found, higher density values could be attributed to the impact of the monsoon. For the linear extension and calcification rates, no significant differences between side and depth were observed. In addition, no correlation with the intensity of internal waves was discovered, which indicates that other environmental factors than internal waves primarily affect growth and calcification of *P. lutea*.

Zusammenfassung

Die Similan Inseln befinden sich in der Nähe des thailändischen Kontinentalschelfs in der Andamansee und sind dem Einfluss von internen Wellen mit großer Amplitude (LAIW oder Solitone) und des Südwest-Monsuns ausgesetzt. Die westliche Seite dieser küstennahen Inselgruppe ist dem Meer zugewandt und wird somit von beiden Phänomenen beeinflusst, wohingegen die östliche Seite der Inseln geschützt ist. Interne Wellen kommen vorrangig in der Tiefe vor und sind dafür bekannt Umweltfaktoren zu verändern, die Auswirkungen auf das Wachstum von Korallen haben. Hingegen verursacht der Monsun vor allem einen höheren Wellengang und verstärkte Sedimentbildung und beeinflusst daher hauptsächlich die oberen Riffbereiche nahe der Wasseroberfläche.

In der vorliegenden Arbeit wird der Einfluss interner Wellen und des Monsuns auf das lineare Wachstum, die Skelettdichte und die Kalkbildung der Steinkoralle *Porites lutea* untersucht. Korallenskelette wurden auf der West- sowie auf der Ostseite der Insel Ko Miang im Zentrum der Similan Inseln in zwei verschiedenen Tiefen (7 m und 20 m) gesammelt. Für die lineare Wachstumsrate wurden Röntgenaufnahmen der jährlichen Dichtebänderung der Korallenskelette verwendet und die fluoreszierenden Bänder analysiert. Die gesamte Skelettdichte, die Mikrodichte und die Porosität der Skelette wurden mit einer speziellen Wägemethode unter Wasser (engl. Buoyant Weighing Method) gemessen. Zudem wurde hierfür das gesamte umschlossene Volumen der Skelette berechnet und das archimedische Prinzip für die Messung des Gesamtvolumens verwendet.

Die Korallenfragmente der Westseite wiesen größere Dichten mit höchsten Werten in einer Tiefe von 7 m auf. Da keine Korrelation der Skelettdichte mit der Intensität der LAIW gefunden wurde, können diese größeren Dichtewerte im Westen dem Einfluss des Monsuns zugeschrieben werden. Es wurden keine Unterschiede der linearen Wachstumsrate und der Kalkbildungsrate auf beiden Seiten der Insel und in den jeweiligen Tiefen gefunden. Zudem bestand keine Korrelation dieser beiden Parameter mit der Intensität der LAIW. Dies deutet darauf hin, dass das Wachstum und die Kalkbildung von *P. lutea* in erster Linie durch andere Umweltfaktoren als die internen Wellen beeinflusst werden.

1 Introduction

Hermatypic (reef-building) scleractinian corals build up a skeleton by the deposition of $CaCO_3$ (calcification) and thus, contribute to the construction of a three-dimensional reef framework (Buddemeier & Kinzie 1976). A regular growth pattern, which is composed of alternating dark and light bands representing differences in the bulk density of the skeletal material, is characteristic of the skeleton of massive scleractinian corals (Knutson *et al.* 1972, Buddemeier & Kinzie 1976).

Corals are affected by physico-chemical environmental factors influencing coral growth and reef development and changes in these factors can alter the annual density banding pattern (Barnes & Devereux 1988, Smith & Buddemeier 1992, Barnes & Lough 1993, Kleypas *et al.* 1999a). In general, variations in the skeletal density can be attributed to seasonal differences in water temperature (Buddemeier *et al*. 1974, Hudson *et al.* 1976, Highsmith 1979), light availability (Knutson *et al.* 1972, Buddemeier *et al.* 1974, Baker & Weber 1975, Highsmith 1979) and the level of sedimentation (Dodge *et al.* 1974, Brown *et al.* 1986).

Most hermatypic corals occur in tropical regions in a relatively narrow range of environmental conditions in warm and well-illuminated surface waters (Achituv & Dubinsky 1990, Lough & Barnes 2000). A positive correlation of water temperature with linear extension and calcification rates has been detected by various studies (Nie *et al.* 1997, Kleypas *et al.* 1999a, Lough & Barnes 2000, Tanzil *et al.* 2009). In addition, reef development may be prevented due to upwelling of cold, nutrient-enriched waters (Stoddart 1973, Birkeland 1988). Because of the efficient internal recycling between the coral and the zooxanthellae symbiont, enhanced nutrient concentrations can have a negative effect on coral growth rates (Birkeland 1988, Muller-Parker & D'Elia 1997).

Light penetration is especially important for the photosynthesis of the symbiotic zooxanthellae and thus, high calcification rates of hermatypic corals can be attributed to the supportive coral symbiosis with the zooxanthellate algae (Pearse & Muscatine 1971, Highsmith 1979, Muscatine 1990). In addition, hydraulic energy can have a negative effect on linear extension rates of corals (Scoffin *et al.* 1992, Riegl 2001). On the other side however, skeletal bulk density has been found to increase along a hydraulic energy gradient, indicating

that this environmental factor is primarily responsible for variations in skeletogenesis of for example *P. lutea* in the Phuket Region, Andaman Sea, Thailand (Scoffin *et al*. 1992).

Moreover, salinity also controls coral growth because fresh water inflow from rivers limits coral development (Achituv & Dubinsky 1990). In addition, high sedimentation is known to cause reductions in linear extension rates and can be a major factor affecting coral growth due to reduced light levels because of turbidity (Dodge *et al.* 1974, Riegl & Bloomer 1995). Finally, carbonate saturation (especially the degree of aragonite saturation), is crucial for the calcification process because calcium carbonate precipitation only occurs in supersaturated waters (Gattuso *et al.* 1998, Kleypas *et al.* 1999b, Ohde & Hossain 2004).

The density banding pattern of hermatypic corals can be used as a record for environmental changes as coral growth rates vary in relation to environmental stress (Knutson *et al.* 1972, Dodge & Vaisnys 1975, Scoffin *et al.* 1992). Most authors agree that high-density (HD) bands are mainly formed during periods of high water temperatures, whereas the formation of low-density (LD) bands can be attributed to seasons with low temperatures (Buddemeier *et al.* 1974, Highsmith 1979, Lough & Barnes 1990). However, Brown *et al.* (1986) question the assumption that two density bands represent one year's growth by reporting asynchronous formation of stress bands in *P. lutea* at Phuket Island (Thailand). They state that dense bands have most likely been deposited asynchronously due to high sedimentation rates resulting in reduced levels of light.

Apart from density bands, annual yellow-green fluorescence bands are formed due to incorporation of terrestrial humic and fulvic acids into the coral skeleton (Isdale 1984, Boto & Isdale 1985, Klein *et al.* 1990, Scoffin *et al.* 1989, Susic *et al.* 1991). Humic and fulvic acids are mainly introduced into the ocean by river discharge and therefore, fluorescent bands can especially be observed in corals from coastal waters (Isdale 1984, Boto & Isdale 1985, Scoffin *et al.* 1989). Thus, the annual fluorescent banding in scleractinian corals can be used to study the terrestrial runoff (Isdale 1984) and brighter fluorescence bands occur due to heavier rainfall during the wet season (Scoffin *et al.* 1989). However, two studies question the presumption that fluorescent bands derive from terrestrial humic and fulvic acids. They assume that fluorescent bands are formed due to breakdown of marine organic matter (Tudhope *et al*. 1996) or that they are linked with skeletal architecture and therefore coincide with the annual density banding pattern (Barnes & Taylor 2001).

In general, high fluorescence bands (HF) coincide with LD skeletal bands, which represent periods of optimum conditions for calcification and are deposited in seasons with high freshwater runoff (Scoffin *et al.* 1989, Klein *et al*. 1990, Barnes & Taylor 2001). Highest coral growth rates (i.e. LD bands) are therefore usually detected during wet seasons with heavy rainfall (Scoffin *et al.* 1989). However, Scoffin *et al.* (1989) have also observed very thin HF bands that coincide with dense skeletal bands. In addition, Scoffin *et al.* (1992) affirm that the deposition of HF bands in *P. lutea* started at the beginning of the dry season (November) and consequently, did not correlate with local rainfall in the Phuket Region, Thailand. These two studies therefore support the finding of Tudhope *et al.* (1996) and Barnes & Taylor (2001) as described above.

The present study has been conducted at the Similan Islands in the Andaman Sea (Thailand), which are influenced by physico-chemical environmental changes due to large amplitude internal waves (LAIW) and monsoon. Internal waves are ubiquitous in the oceans and occur between separate layers of density stratification within the water column due to differences in temperature and salinity (Osborne & Burch 1980, Leichter *et al.* 2005, Roder *et al.* 2010). In the Andaman Sea, internal waves are tidally generated northwest of Sumatra and at the Andaman and Nicobar Islands and travel through the Andaman basin (Perry & Schimke 1965, Osborne & Burch 1980, Jackson 2004). When they reach shallow waters, they bring up cold, nutrient-enriched water from below the pycnocline (Vlasenko & Stashchuk 2007, Schmidt *et al.* 2012, Wall *et al.* 2012). Therefore, they may have an important, yet so far mainly unknown impact on the development of coral reefs and coral growth (Wall *et al.* 2012, Schmidt & Richter 2013).

In the Andaman Sea, LAIW with extraordinary large amplitudes of more than 60 meters and current speeds of up to 2 m s^{-1}, travelling in packets of five to eight waves, have been observed (Perry & Schimke 1965, Osborne & Burch 1980, Jackson 2004). The occurrence of internal waves can especially be detected by large temperature fluctuations, as the temperature drops suddenly (within minutes) up to 10 °C (Leichter & Miller 1999, Leichter *et al.* 2003, Schmidt *et al.* 2012). Additionally, the nutrient concentration increases and the pH (i.e. Ω_{arag}) declines due to the entrainment of the deep waters into shallow areas (Osborne & Burch 1980, Roder *et al.* 2010, Roder *et al.* 2011, Schmidt *et al.* 2012).

In addition, the Andaman Sea is subject to a monsoonal climate with a dry northeast (NE, November – March) and a wet southwest (SW) monsoon (April – October) with intense seasonal rainfall, strong winds and heavy swell (Scoffin *et al.* 1992). The main effects of the SW monsoon on coral reefs are turbulent mixing and increased sedimentation (Wall *et al*. 2012). The chain of the Similan Islands is located almost perpendicular to the impact of LAIW and SW monsoon, since both reach the islands from the west (W) (Jackson 2004, Schmidt *et al.* 2012). In contrast, the east (E) side of the islands is sheltered from both events. Therefore, the spatial impact of both phenomena is coupled, whereas they are temporally separated. LAIW have their strongest impact during the dry season (NE monsoon) due to a shallow pycnocline (Brown 2007, Schmidt *et al.* 2012). On the contrary, highest surface waves have been observed during the wet season (SW monsoon) because of prevailing strong winds (Wall *et al.* 2012).

While LAIW especially influence greater depth, the monsoon has an impact on shallow slope areas. At the Similan Islands, the impact of LAIW on scleractinian corals declines accordingly from exposed W deep to shallow waters, followed by sheltered E deep and shallow sites (Roder *et al.* 2011). In addition, highest temperature fluctuations (a proxy for LAIW) can be observed at the west side with increasing depths from February until April leading to the assumption that LAIW-intensity peaks in spring (Schmidt *et al.* 2012, Wall *et al.* 2012, Schmidt & Richter 2013). Therefore, coral reef development only occurs at the east side of the islands, whereas the ocean facing, west side lacks an actual reef framework due to more intense upwelling and wave action (Schmidt 2010, Schmidt *et al.* 2012, Wall *et al.* 2012). Hence, the positive correlation of LAIW with depth is likely responsible for the reduced framework at deeper depths (Schmidt *et al.* 2012). Reduced growth of *P. lutea* was also found at W 20 m due to the unfavourable environmental conditions originating from LAIW (Schmidt & Richter 2013). In contrast, the monsoon exposure had no negative effect on coral growth (Schmidt & Richter 2013).

The aim of the present study is to investigate if LAIW and monsoon exposure have an effect on growth rate, skeletal density and calcification rate of the scleractinian coral *Porites lutea*, the predominant reef-building coral at the Similan Islands (Brown 2007). For this purpose, the linear extension rate, the skeletal density and the calcification rate of coral skeletons from LAIW-exposed and -sheltered sample sites are compared. It is hypothesised that the linear

extension rate of *P. lutea* is reduced at the exposed west side compared to the sheltered east due to the impact of LAIW and monsoon from west. It is further assumed that coral growth is significantly reduced at 20 m compared to 7 m depth because of the higher impact of LAIW at depth. In addition, the stronger intensity of internal waves and monsoon at west is expected to cause greater skeletal densities in the respective *P. lutea* samples.

2 Material and methods

2.1 Study site and coral sampling

Nubbins of the massive scleractinian coral *Porites lutea* (Milne Edwards & Haime 1851) were collected at Ko Miang Island, which belongs to the Similian Islands, an archipelago in the Andaman Sea located 60 km off the Thai coast (Fig. 1). Each mother colony was sampled by chiselling one nubbin per colony from the central upper part of the coral head, using scuba. A total of 50 nubbins was sampled at the west (W) and east (E) side of the island at two different depths (W 20 m: 12 nubbins, W 7 m: 11 nubbins, E 20 m: 15 nubbins, E 7 m: 12 nubbins). The coral samples were collected in March 2008 and bleached to remove the organic tissue.

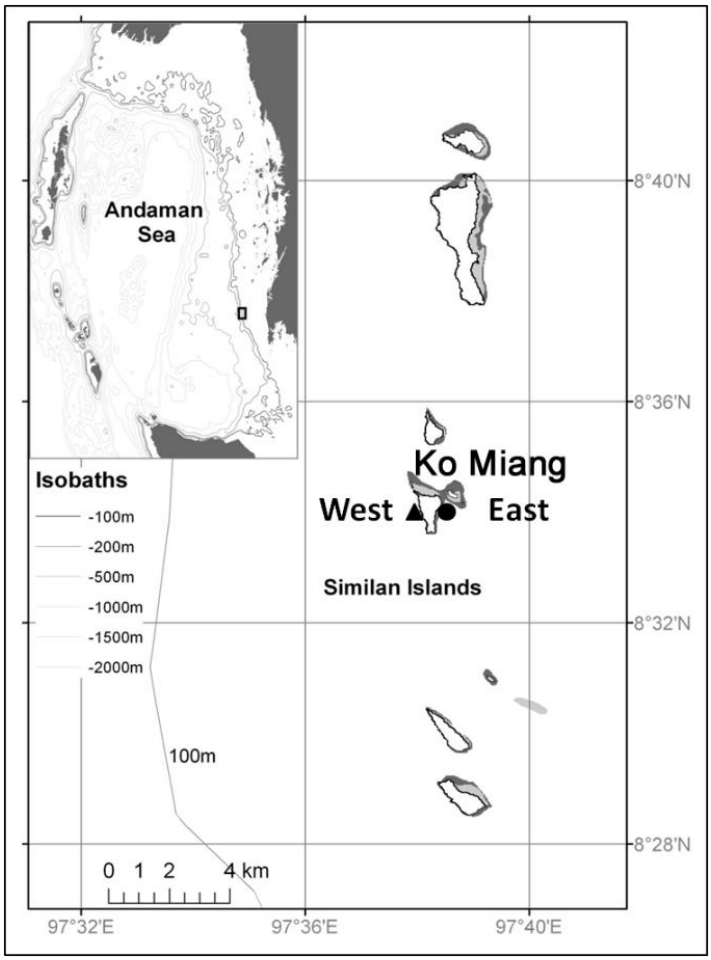

Figure 1. Map of the Andaman Sea off the coast of Thailand. Similan Islands in the east and the Andaman-Nicobar Islands in the west (small map). Main map: Close-up of the box on the small map with the 9 Similan Islands. Sample sites at the LAIW- and monsoon-exposed west and sheltered east side at the central Similan island Ko Miang are marked. (Figure from Schmidt *et al.* 2012, modified after Jackson 2004)

2.2 Linear extension rate

X-radiography and fluorescence analyses were applied to investigate the linear extension rate by analysing the annual banding pattern of the coral nubbins. Density bands are revealed in coral slabs that have been cut along the major growth axis and examined by X-radiography. X-radiographs show the alternating banding pattern of high-density (HD) and low-density (LD) bands. The growth increment of one year is usually represented by one pair of density bands in the coral skeleton (Fig. 2, Knutson *et al.* 1972, Buddemeier *et al.* 1974, Buddemeier & Kinzie 1976). Due to the circumstance that the density banding pattern follows an annual sequence, it is possible to determine annual linear extension rates by means of X-radiographic studies of the skeleton (Knutson *et al.* 1972, Baker & Weber 1975, Barnes & Devereux 1988).

In addition, annual fluorescent bands appear in massive corals by illumination with ultra violet (UV) light (Fig. 3, Isdale 1984). While X-radiographic images display the density of the whole fragment, the fluorescence method only shows the banding pattern on the surface of the coral slab. Both methods were applied for this study because depending on the fragment and the cut surface of the individual slabs, the possibility to detect the banding pattern differs between the two methods.

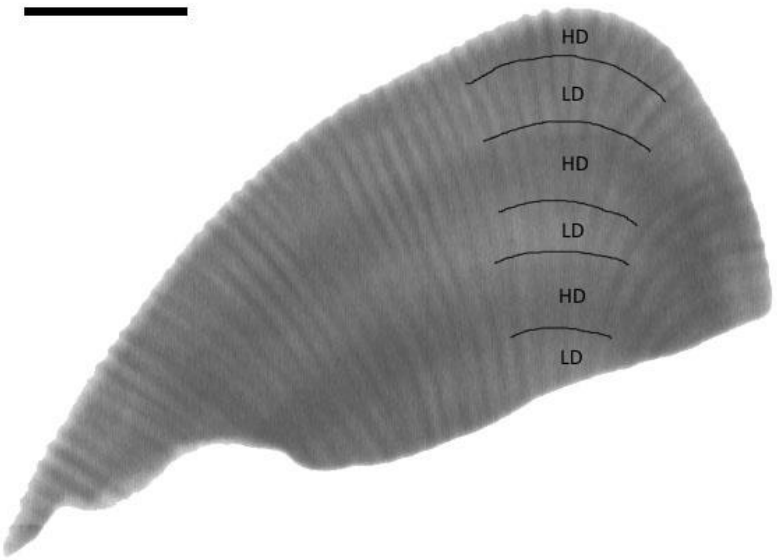

Figure 2. Example of X-radiograph picture of *Porites lutea* collected at the west side of Ko Miang Island at 7 m depth. The coral slab has been cut along the major growth axis. The lines highlight the transition between high-density (HD) and low-density (LD) bands indicating the banding pattern over 2 years. The scale represents 10 mm.

In total, 49 coral skeletons were used (W 20 m: 12, W 7 m: 11, E 20 m: 14, E 7 m: 12). One skeleton sample from E 20 m was excluded from the examination, as the different density bands were not sufficiently visible. Therefore, this coral was also excluded from the calculation of the calcification rate, but was used to detect the skeletal density and porosity. Coral nubbins were cut along the major growth axis in 7-8 mm thick slabs using a FKS/E Proxxon stand saw with a diamond blade (85 x 0.9 mm). The slabs were then rinsed in deionised water in an ultrasonic bath (Bandelin SONOREX RK 510) for one minute to remove remaining particles from the pores. Afterwards, they were dried in a compartment dryer at 45°C for 24 hours. The X-radiography was conducted with automatic settings (approx. 80 kV and 3.5 mA for 4-5 minutes) and the positives of the X-radiographs were digitalised automatically (Fig. 2).

For the analysis of the fluorescence banding, a black-light lamp mounted on a frame was used. The pictures were taken in a darkened room to shield the setup from surrounding illumination. The coral slabs were placed underneath the source of ultraviolet (UV) light at a distance of approximately 15 cm to ensure a uniform and sufficient illumination. A Canon G 12 digital compact camera was mounted on a tripod and set for macro shootings. Pictures of each coral slab were taken with and without a yellow filter, which resulted in photographs with a yellow-grey banding pattern or light and dark blue bands respectively (Fig. 3).

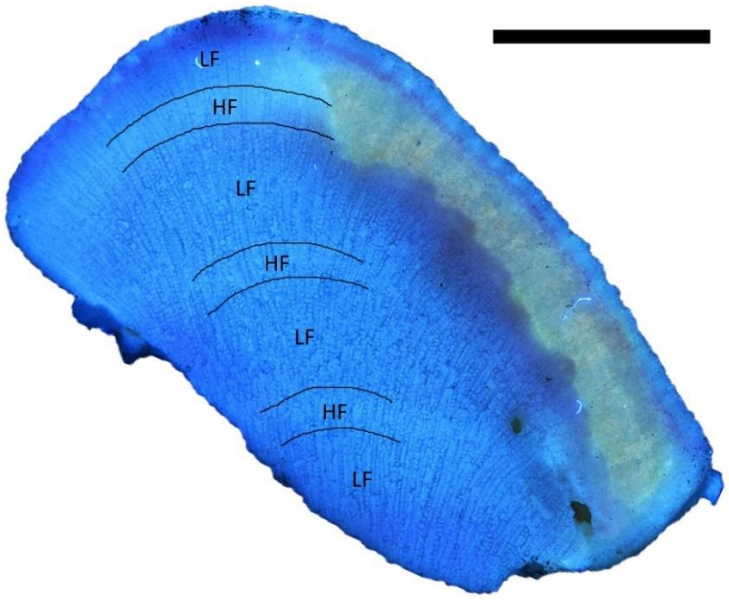

Figure 3. Example of fluorescence image of *Porites lutea* collected at the east side of Ko Miang Island at 20 m depth. The coral slab has been cut along the major growth axis and was illuminated with ultraviolet (UV) light. The lines highlight the transition between high fluorescence (HF) and low fluorescence (LF) bands. The scale represents 10 mm.

Depending on the picture quality and visibility of the banding, either the pictures with or without the yellow filter were used for the analysis. In the literature (e.g. Isdale 1984, Klein *et al.* 1990, Scoffin *et al.* 1989, Susic *et al.* 1991), yellow-green fluorescence bands are usually used for fluorescence analysis. In the present study however, the banding was in most cases more clearly recognisable on pictures with light and dark blue bands. The brightness and contrast of the X-radiography and fluorescence pictures were edited manually in order to be able to identify the banding with the highest possible precision.

Both X-ray and fluorescence pictures were further processed to the same size and the X-radiograph was placed on top of the fluorescence picture of the same coral nubbin using the programme *Adobe Photoshop Elements 6.0*. The pictures were scaled and the X-ray image cut along three individual polyps close to the major growth axis so that the fluorescence image underneath became visible on half of the picture making it possible to simultaneously use both methods for the analysis of the banding pattern (Fig. 4). The width of the bands was measured with the programme *ImageJ – Image Processing and Analysing in Java* by measuring their distance in pixels. The thickness of the individual bands was determined by setting a mark at the transition point between two bands along the growth axis of each of the three polyps. In nubbins, where the banding pattern varied slightly between X-ray and fluorescence picture, the picture showing the clearer banding was used. Density bands of all three selected polyps of each coral nubbin were marked. By using the x- and y-coordinates of each mark detected by *ImageJ*, the thickness of the single bands was determined and the linear extension rate calculated for each polyp and coral nubbin.

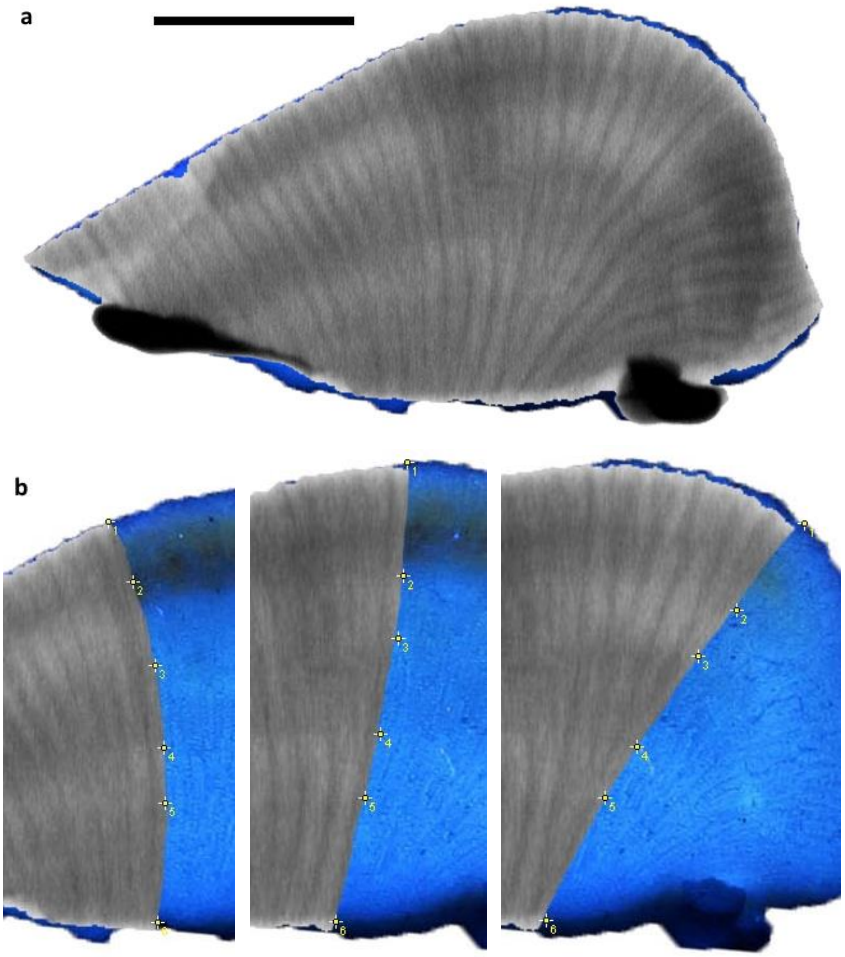

Figure 4. Example of combined X-radiograph and fluorescence image of a *Porites lutea* nubbin collected at the west side of Ko Miang Island at 20 m depth. (a) Combined picture used to determine the annual linear growth rate. (b) X-radiograph cut along three individual polyps close to the major growth axis. Yellow marks represent transition points between two bands. Scale represents 10 mm.

2.3 Skeletal density and porosity

Three parameters were measured in order to determine the skeletal density: skeletal bulk density, micro-density and porosity. The term skeletal bulk density (g/cm^3) is defined as the mass (dry weight) divided by the total enclosed volume of the coral (including the volume of the skeletal voids, Bucher *et al.* 1998). The bulk density is inversely related to porosity (%), which is defined as the volume of the skeletal voids in relation to the total enclosed volume (Bucher *et al.* 1998). In contrast to the bulk density, micro-density (g/cm^3) describes the density of the carbonate skeleton (i.e. the gravity of the skeletal material, Bucher *et al.* 1998).

The X-radiographic image of each nubbin was used to identify the maximum growth axis on the coral slab. This part was marked on each nubbin and cut out with a FKS/E Proxxon stand saw (diamond blade, 85 x 0.9 mm), resulting in quadratic sticks of 7-8 mm width and different

lengths of 15-40 mm (depending on the size of the respective coral nubbin). The sticks were rinsed in deionised water in an ultrasonic bath (Bandelin SONOREX RK 510) for one minute and dried in a compartment dryer at 45°C for 24 hours.

The nubbins were bleached again for 2 days using a 10% solution of commercial bleach (Dan Klorix) to remove any remained rest of organic material. Afterwards the nubbins were soaked in distilled water and any possible air bubbles were removed from the inner and outer skeleton by pumping distilled water through the nubbins with a syringe. By doing so, any residual traces of tissue were removed from the skeleton and distilled water was filled into the skeletal voids. The nubbins remained in distilled water for three days to ensure that they were completely soaked. Before the corals were weighed, the distilled water was changed again.

The buoyant weighing technique described by Davies (1989) was used. Skeletal micro- and bulk density, as well as porosity of each *P. lutea* nubbin were determined from the different weight and volume determinations after Bucher *et al.* (1998). For this, a precise electronic balance (model) reading to 0.00001 g was mounted on a platform above a small aquarium. The nubbins were then weighed underwater on a watch glass (diameter = 7 cm) in a nylon net attached to the underside of the balance by three nylon strands. The watch glass was covered with 5 cm of distilled water and one coral nubbin at a time was put in the weighing chamber at least 5 minutes before they were weighed to ensure temperature adaptation. Before the weighing process, distilled water was again pumped through each nubbin with the help of a syringe and remaining air bubbles at the outside of the nubbins were removed with a fine paintbrush. The temperature of the distilled water was monitored during the whole weighing process and changes of 0.1°C and more were noted to ensure that the correct density of the water was used for each calculation. The density of distilled water, at variable temperatures between 21 and 23 °C, was obtained from Tilton & Taylor (1937). After the buoyant weight was obtained, the coral skeletons were dried overnight to constant weight at 60°C and their dry weight was determined with the same balance.

In order to calculate the total enclosed volume (volume of skeleton and skeletal voids), the dry sticks were coated with a thin layer of paraffin wax to inhibit the skeletal voids to be filled with the weighing medium. Sewing thread was tied around each coral stick and the stick quickly dipped into molten wax at 105-110°C. Afterwards, it was immediately moved around

in the air to prevent the formation of drops on the outside of the skeletal stick and to ensure a uniform wax coating. The coated stick was hung to dry and the thread cut close to the skeleton. The dry and buoyant weight of the waxed coral was determined and attention payed to only submerge the coral sticks for a short period of time during the weighing process to prevent water penetrating into the skeletal voids (despite the wax coating). In most cases, no air bubbles were detected during the weighing. For the few cases in which air bubbles emerged on the outside of the nubbin due to an incomplete wax coating, the first value, which was stable for a few seconds, was noted. The equations from Bucher *et al.* (1998) were used for the calculation of the micro-density, bulk density and porosity.

2.4 Calcification rate

The annual calcification rate of each coral nubbin (g x cm^{-2} x yr^{-1}) was determined by multiplying the average annual linear extension rate (mm x yr^{-1}) by the skeletal bulk density (g x cm^{-3}).

2.5 Environmental data

An index in degree-days cooling (DDC in [°C d]) was calculated for the intensity and frequency of LAIW (for the calculation and definition see Schmidt & Richter 2013; temperature data for March 2007 to November 2008 were provided by Schmidt unpubl.). This LAIW-index was used for correlation analyses for the linear extension rate, skeletal density (skeletal bulk density, micro-density and porosity) and calcification rate.

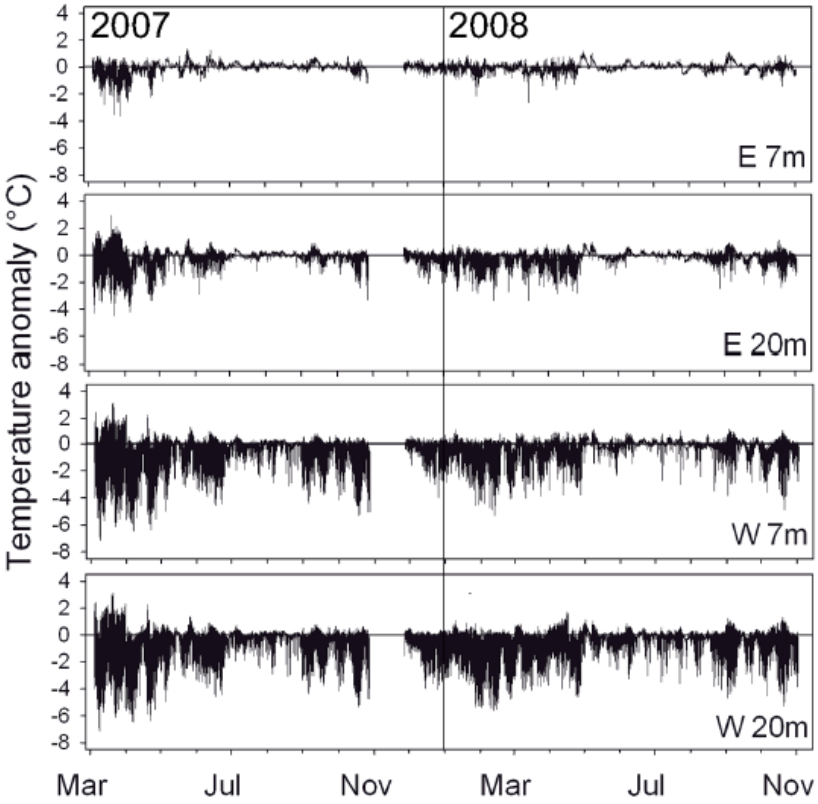

Figure 5. Temperature anomalies at Ko Miang, Similan Islands. Period: March 2007 to November 2008, gap in data due to exceeded storage capacity. For calculation of temperature anomalies relative to mode values see Schmidt & Richter (2013). (Figure from Schmidt & Richter 2013)

2.6 Statistical analysis

For the statistical analysis, the software *SigmaPlot 11.0* was used. The data were tested for normal distribution (Shapiro-Wilk Test) and for equal variance. A Two Way ANOVA (Analysis of Variance) was used to test for the main effect of the two independent factors side (W and E) and depth (7 and 20 m) and the interaction between both factors on skeletal bulk density, micro-density and porosity. The Holm-Sidak Test was used for pairwise multiple comparisons for each factor. In addition, a One Way ANOVA was used to test each factor separately for significant differences. As the normality test failed for the factor side of the micro-density, the non-parametric Kruskal-Wallis test (ANOVA on Ranks) was used. The linear extension rate and the calcification rate did not meet the normality assumptions. Therefore, the non-parametric Kruskal-Wallis test (ANOVA on Ranks) was used for these two parameters. For correlation analyses, linear regressions were used to test the different parameters for a correlation with the LAIW-index.

3 Results

3.1 Linear extension rate

Linear extension rates of *Porites lutea* revealed no statistically detectable differences between side (W and E) and depth (7 and 20 m), despite supposed lower values at the deep compared to the shallower sites (Tab. 4, Fig. 6, Kruskal-Wallis ANOVA: p = 0.152).

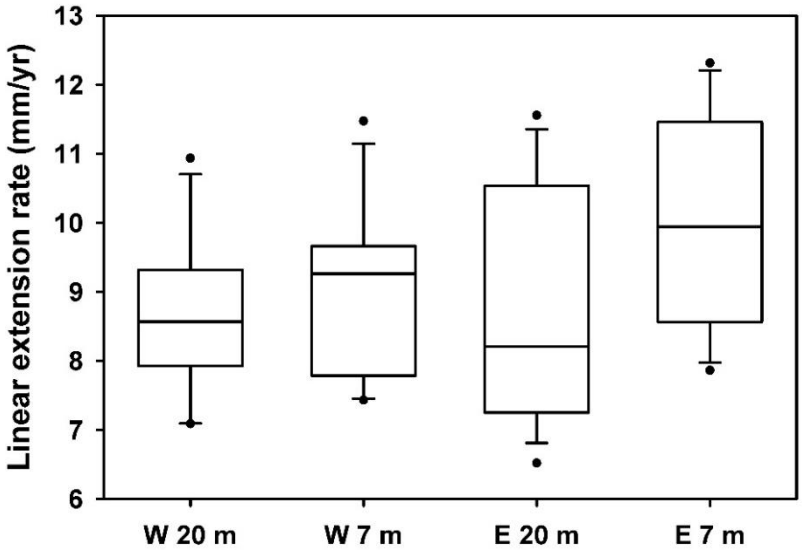

Figure 6. Central tendency box plots (median with 25th and 75th percentile and non-outlier range) with extremes (dots) of linear extension rate (mm/yr) of *Porites lutea* plotted against all sample sites at the central Similan island Ko Miang (west (W) = exposed to LAIW and monsoon, east (E) = sheltered from LAIW and monsoon in 20 m and 7 m depth).

3.2 Skeletal density and porosity

Skeletal bulk densities of *P. lutea* showed a statistically significant interaction between side (W and E) and depth (7 and 20 m, Two Way ANOVA: p = 0.049) with higher density values at the exposed W compared to the sheltered E (Tab. 1, Fig. 7, Holm-Sidak Test: p = 0.017, One Way ANOVA: p = 0.026) and higher values at W 7 m compared to E 7 m (Holm-Sidak Test: p = 0.004).

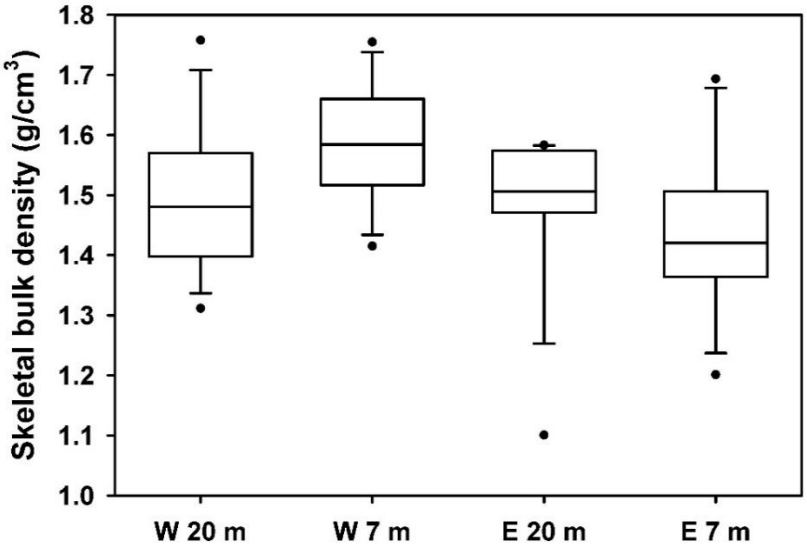

Figure 7. Central tendency box plots (median with 25th and 75th percentile and non-outlier range) with extremes (dots) of skeletal bulk density (g/cm^3) of *Porites lutea* plotted against all sample sites at the central Similan island Ko Miang (west (W) = exposed to LAIW and monsoon, east (E) = sheltered from LAIW and monsoon in 20 m and 7 m depth).

Table 1. Two Way Analysis of Variance (ANOVA), Holm-Sidak Test and One Way ANOVA for skeletal bulk density of *Porites lutea* from all sample sites of the central Similan island Ko Miang. Treatment factors: side (W versus E) and depth (7 m versus 20 m), pairwise multiple comparisons via Holm-Sidak Test, One Way ANOVA to test factors separately, df = degrees of freedom, SS = sum of squares, MS = means square, F = F-value, p = significance level.

Test	Factor	P	df	SS	MS	F
Two Way ANOVA	Side	0.017	1	0.0863	0.0863	6.114
	Depth	0.419	1	0.00936	0.00936	0.664
	Side x depth	0.049	1	0.0578	0.0578	4.093
	Residual		46	0.649	0.0141	
	Total		49	0.791	0.0161	
Holm-Sidak Test	Side	0.017				
	Depth	0.419				
	Depth within W	0.059				
	Depth within E	0.379				
	Side within 7 m	0.004				
	Side within 20 m	0.743				
One Way ANOVA	Side	0.026	1	0.0780	0.0780	5.253
	Residual		48	0.713	0.149	
	Total		49	0.791		
	Depth	0.492	1	0.00782	0.00782	0.479
	Residual		48	0.783	0.0163	
	Total		49	0.791		

The micro-density of *P. lutea* showed a statistically significant interaction between side (W and E) and depth (7 and 20 m, Two Way ANOVA: p = 0.043) with higher density values at 7 m than at 20 m depth (Tab. 2, Fig. 8, Holm-Sidak Test and One Way ANOVA: p < 0.001). Higher values were further found at E 7 m compared to E 20 m (Holm-Sidak Test: p < 0.001) and at E 7 m compared to W 7 m (Holm-Sidak Test: p = 0.027).

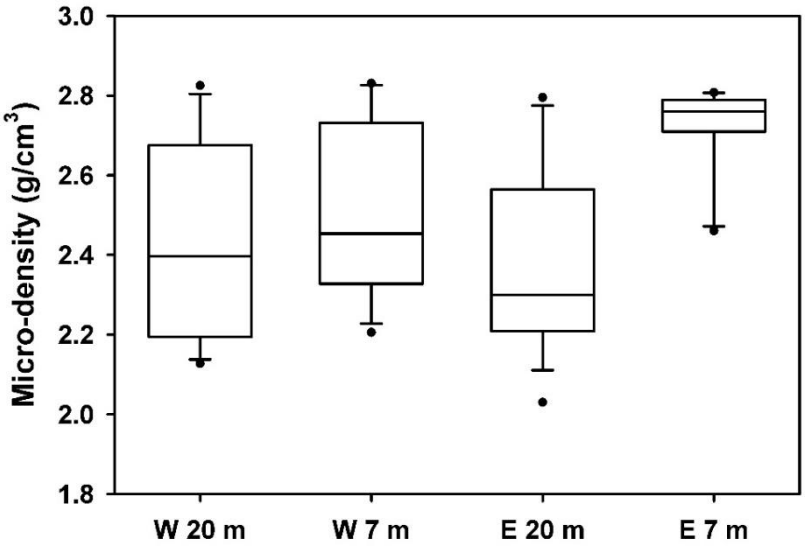

Figure 8. Central tendency box plots (median with 25th and 75th percentile and non-outlier range) with extremes (dots) of micro-density (g/cm^3) of *Porites lutea* plotted against all sample sites at the central Similan island Ko Miang (west (W) = exposed to LAIW and monsoon, east (E) = sheltered from LAIW and monsoon in 20 m and 7 m depth).

Table 2. Two Way Analysis of Variance (ANOVA), Holm-Sidak Test, One Way ANOVA and Kruskal-Wallis Test for micro-density of *Porites lutea* from all sample sites of the central Similan island Ko Miang. Treatment factors: side (W versus E) and depth (7 m versus 20 m), pairwise multiple comparisons via Holm-Sidak Test, One Way ANOVA to test factors separately, df = degrees of freedom, SS = sum of squares, MS = means square, F = F-value, p = significance level.

Test	Factor	P	df	SS	MS	F
Two Way ANOVA	Side	0.209	1	0.0706	0.0706	1.624
	Depth	<0.001	1	0.564	0.564	12.966
	Side x depth	0.043	1	0.188	0.188	4.316
	Residual		46	1.999	0.0435	
	Total		49	2.847	0.0581	
Holm-Sidak Test	Side	0.209				
	Depth	<0.001				
	Depth within W	0.304				
	Depth within E	<0.001				
	Side within 7 m	0.027				
	Side within 20 m	0.558				
Kruskal-Wallis Test	Side	0.442				
One Way ANOVA	Depth	<0.001	1	0.605	0.605	12.954
	Residual		48	2.242	0.0467	
	Total		49	2.847		

The porosity of *P. lutea* showed a statistically significant interaction between side (W and E) and depth (7 and 20 m, Two Way ANOVA: p = 0.012), with higher density values at the sheltered E compared to the exposed W (Tab. 3, Fig. 9, Holm-Sidak Test: p = 0.026). Higher values were determined at E 7 m compared to E 20 m (Tab. 3, Fig. 9, Holm-Sidak Test: p = 0.002) and at E 7 m compared to W 7 m (Holm-Sidak Test: p = 0.002).

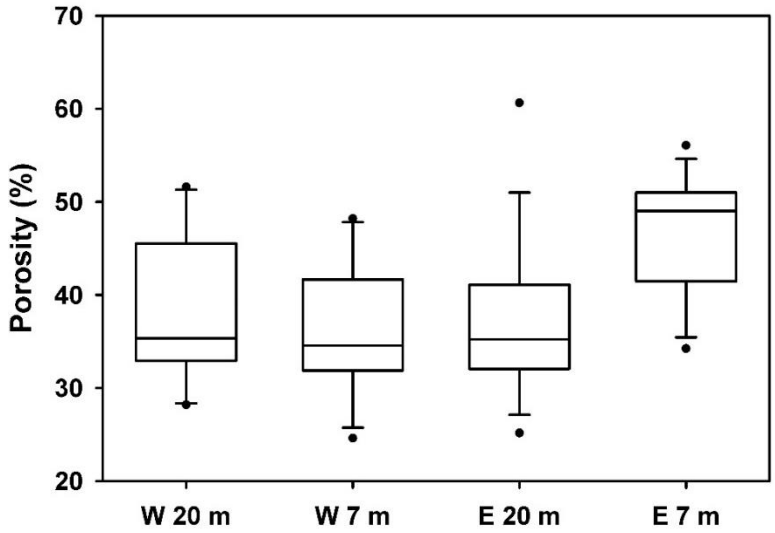

Figure 9. Central tendency box plots (median with 25th and 75th percentile and non-outlier range) with extremes (dots) of porosity (%) of *Porites lutea* plotted against all sample sites at the central Similan island Ko Miang (west (W) = exposed to LAIW and monsoon, east (E) = sheltered from LAIW and monsoon in 20 m and 7 m depth).

Table 3. Two Way Analysis of Variance (ANOVA), Holm-Sidak Test and One Way ANOVA for porosity of *Porites lutea* from all sample sites of the central Similan island Ko Miang. Treatment factors: side (W versus E) and depth (7 m versus 20 m), pairwise multiple comparisons via Holm-Sidak Test, One Way ANOVA to test factors separately, df = degrees of freedom, SS = sum of squares, MS = means square, F = F-value, p = significance level.

Test	Factor	P	df	SS	MS	F
Two Way ANOVA	Side	0.026	1	300.416	300.416	5.318
	Depth	0.061	1	208.594	208.594	3.693
	Side x depth	0.012	1	383.598	383.598	6.791
	Residual		46	2598.335	56.486	
	Total		49	3473.000	70.878	
Holm-Sidak Test	Side	0.026				
	Depth	0.061				
	Depth within W	0.643				
	Depth within E	0.002				
	Side within 7 m	0.002				
	Side within 20 m	0.827				
One Way ANOVA	Side	0.067	1	236.608	236.608	3.509
	Residual		48	3236.392	67.425	
	Total		49	3473.000		
	Depth	0.066	1	237.853	237.853	3.529
	Residual		48	3235.147	67.399	
	Total		49	3473.000		

3.3 Calcification rate

Calcification rates of *Porites lutea* revealed no statistically detectable differences between side (W and E) and depth (7 and 20 m), despite supposed lower values at the deep compared to the shallower sites (Tab. 4, Fig. 10, Kruskal-Wallis ANOVA: p = 0.373).

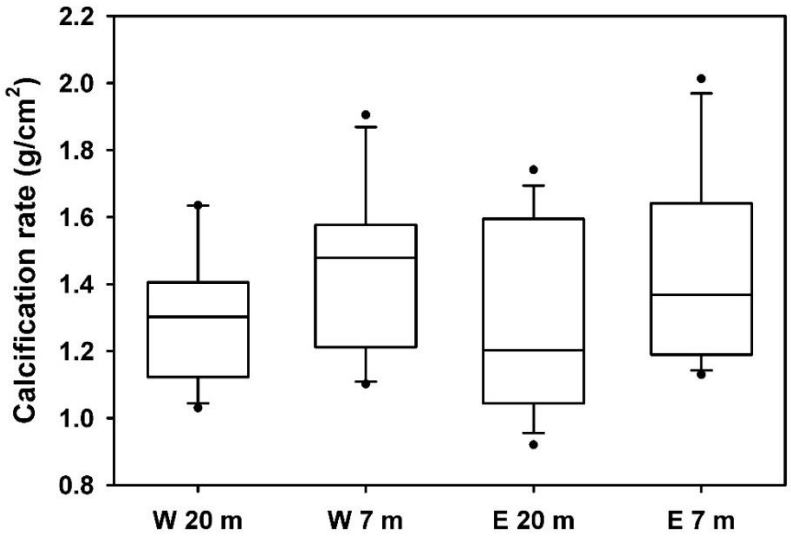

Figure 10. Central tendency box plots (median with 25th and 75th percentile and non-outlier range) with extremes (dots) of calcification rate (g/cm^2) of *Porites lutea* plotted against all sample sites at the central Similan island Ko Miang (west (W) = exposed to LAIW and monsoon, east (E) = sheltered from LAIW and monsoon in 20 m and 7 m depth).

Table 4. Linear extension rate (mm/yr), skeletal bulk density (g/cm^3) and calcification rate (g/cm^2) of *Porites lutea* displayed for all sample sites (W = west, E = east) and depths (7 and 20 m) at the central Similan island Ko Miang. All values given as mean ± standard deviation (SD).

Sample site	Linear extension rate (mm/yr)	Skeletal bulk density (g/cm^3)	Calcification rate (g/cm^2)
W 20 m	8.696 ± 1.084	1.494 ± 0.113	1.299 ± 0.188
W 7 m	8.997 ± 1.161	1.590 ± 0.090	1.435 ± 0.237
E 20 m	8.791 ± 1.703	1.478 ± 0.118	1.294 ± 0.278
E 7 m	9.930 ± 1.432	1.437 ± 0.129	1.431 ± 0.274

3.4 Correlation with LAIW-index

Scatter plots were created for linear extension rate, skeletal density (bulk density, micro-density and porosity) and calcification rate of *P. lutea* plotted against the LAIW-index in degree-days cooling (DDC). Despite the fact that all parameters (linear extension: Fig. 11, skeletal bulk density: Fig. 12, micro-density: Fig. 13, porosity: Fig. 14, and calcification rate: Fig. 15) showed decreasing values with increasing LAIW-intensity, none of them revealed a statistically significant correlation with DDC (Tab. 5).

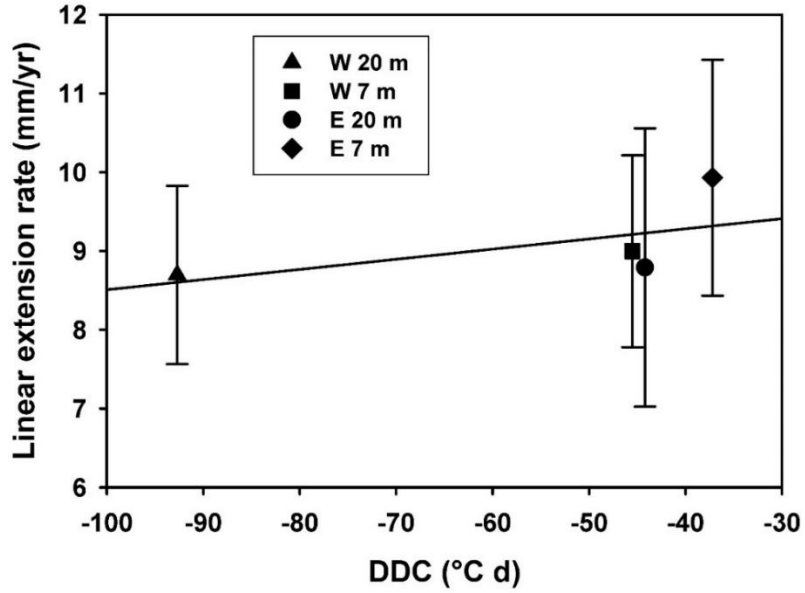

Figure 11. Scatter plot with mean values ± standard deviation (error bars) and linear regression line of linear extension rate (mm/yr) of *Porites lutea* plotted against the LAIW-index (in degree-days cooling = DDC in [°C d]) from all sample sites at the central Similan island Ko Miang (west (W) = exposed to LAIW and monsoon, east (E) = sheltered from LAIW and monsoon in 20 m and 7 m depth; correlation coefficient of regression line $r^2 = 0.037$, $p = 0.186$).

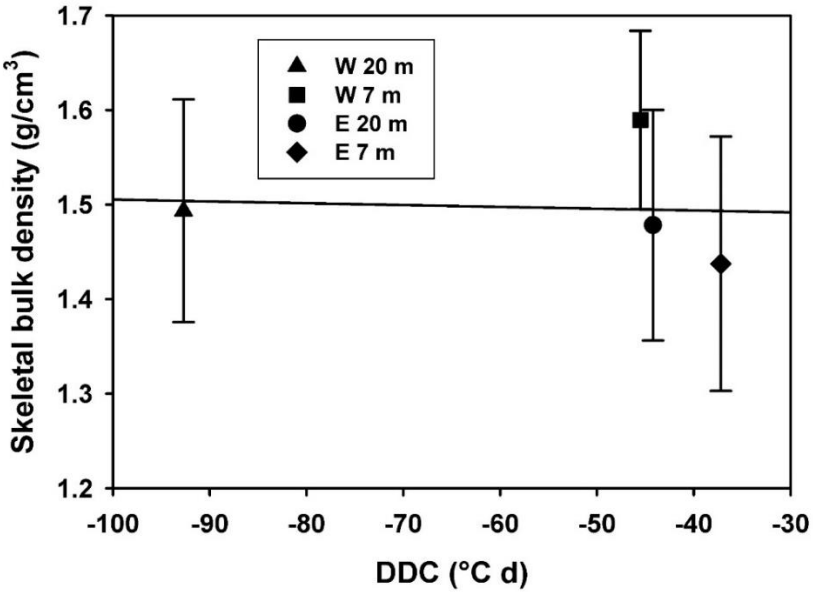

Figure 12. Scatter plot with mean values ± standard deviation (error bars) and linear regression line of skeletal bulk density (g/cm^3) of *Porites lutea* plotted against the LAIW-index (in degree-days cooling = DDC in [°C d]) from all sample sites at the central Similan island Ko Miang (west (W) = exposed to LAIW and monsoon, east (E) = sheltered from LAIW and monsoon in 20 m and 7 m depth; correlation coefficient of regression line $r^2 = 0.001$, $p = 0.820$).

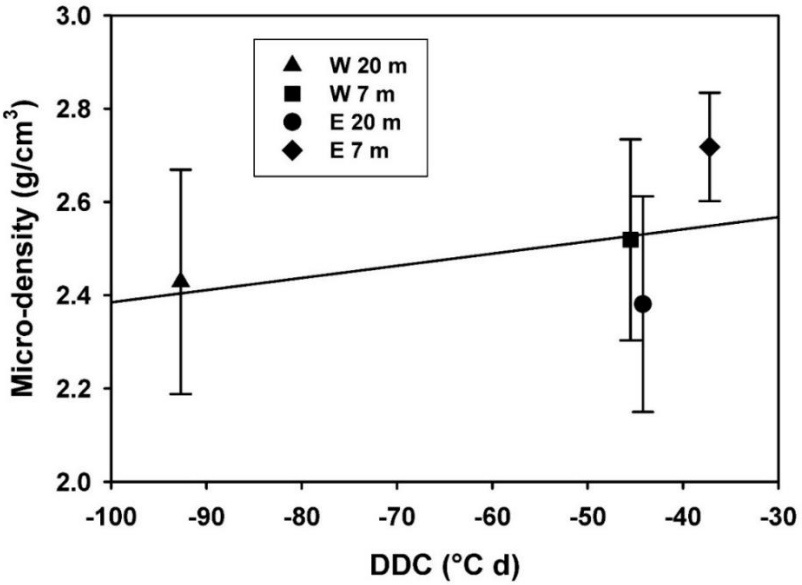

Figure 13. Scatter plot with mean values ± standard deviation (error bars) and linear regression line of micro-density (g/cm^3) of *Porites lutea* plotted against the LAIW-index (in degree-days cooling = DDC in [°C d]) from all sample sites at the central Similan island Ko Miang (west (W) = exposed to LAIW and monsoon, east (E) = sheltered from LAIW and monsoon in 20 m and 7 m depth; correlation coefficient of regression line $r^2 = 0.056$, $p = 0.097$).

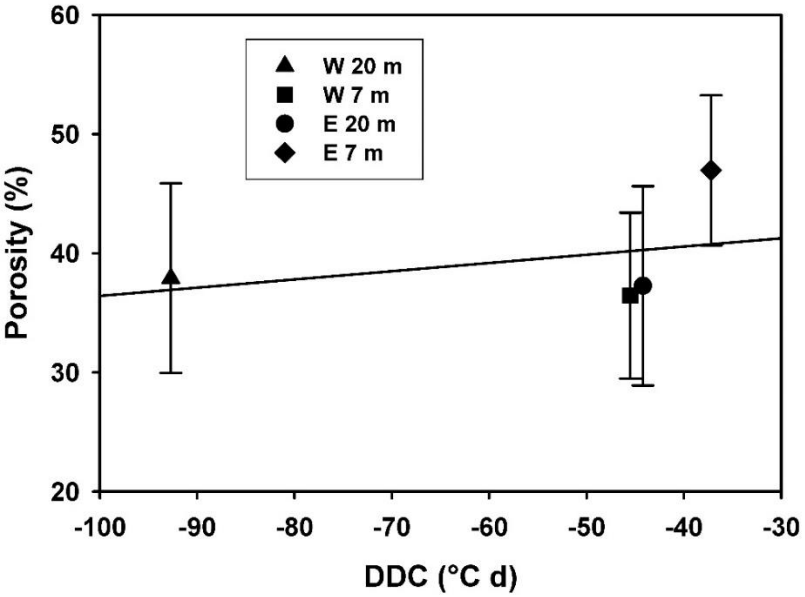

Figure 14. Scatter plot with mean values ± standard deviation (error bars) and linear regression line of porosity (%) of *Porites lutea* plotted against the LAIW-index (in degree-days cooling = DDC in [°C d]) from all sample sites at the central Similan island Ko Miang (west (W) = exposed to LAIW and monsoon, east (E) = sheltered from LAIW and monsoon in 20 m and 7 m depth; correlation coefficient of regression line $r^2 = 0.032$, $p = 0.211$).

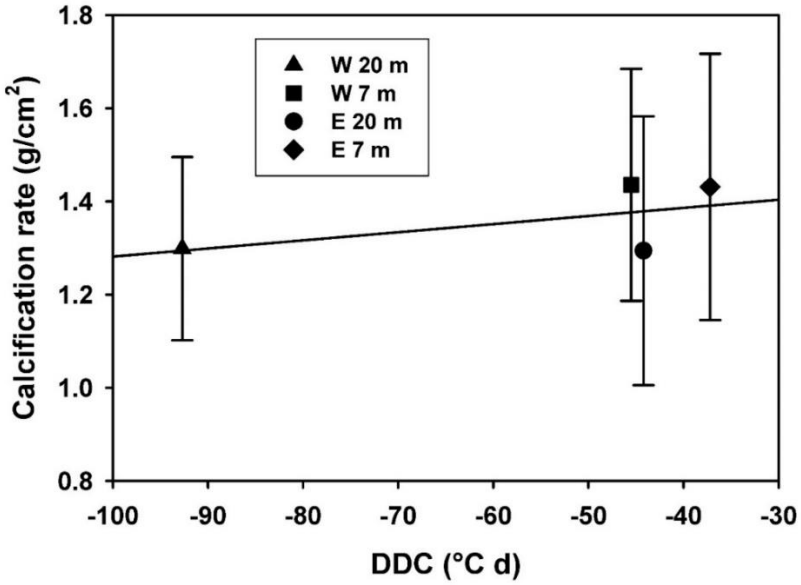

Figure 15. Scatter plot with mean values ± standard deviation (error bars) and linear regression line of calcification rate (g/cm^2) of *Porites lutea* plotted against the LAIW-index (in degree-days cooling = DDC in [°C d]) from all sample sites at the central Similan island Ko Miang (west (W) = exposed to LAIW and monsoon, east (E) = sheltered from LAIW and monsoon in 20 m and 7 m depth; correlation coefficient of regression line $r^2 = 0.022$, $p = 0.311$).

Table 5. Analysis of Variance (ANOVA) of linear regression of linear extension rate, skeletal bulk density, micro-density, porosity and calcification rate of *Porites lutea* with LAIW-index (in degree-days cooling = DDC in [°C d]) from all sample sites of the central Similan island Ko Miang. (For calculation of DDC see Schmidt & Richter 2013, temperature data for DDC provided by Schmidt unpubl.)

Parameter	Factor	P	df	SS	MS	F	R^2
Linear extension rate	Regression	0.186	1	3.900	3.900	1.798	0.037
	Residual		47	101.929	2.169		
	Total		48	105.830	2.205		
Skeletal bulk density	Regression	0.820	1	0.000858	0.000858	0.0521	0.001
	Residual		48	0.790	0.0165		
	Total		49	0.791	0.0161		
Micro-density	Regression	0.097	1	0.160	0.160	2.862	0.056
	Residual		48	2.686	0.0560		
	Total		49	2.847	0.0581		
Porosity	Regression	0.211	1	112.595	112.595	1.608	0.032
	Residual		48	3360.405	70.008		
	Total		49	3473.000	70.878		
Calcification rate	Regression	0.311	1	0.0712	0.0712	1.050	0.022
	Residual		47	3.187	0.0678		
	Total		48	3.258	0.0679		

4 Discussion

In the present study, the determination of linear extension rates, skeletal density and calcification rates of *Porites lutea* in relation to LAIW-impact were examined. The study revealed no correlation of these parameters with frequency and intensity of internal waves at the central Similan island Ko Miang. Due to upwelling of deep water, internal waves alter environmental factors such as temperature, nutrient concentration and pH that influence coral growth. Higher skeletal bulk densities were determined at the west side of the island, which is exposed to LAIW and the monsoon, and especially at 7 m depth compared to 20 m. In contrast, linear extension and calcification rates did not show significant differences between the two sides of the island (W and E) and the two depths (7 and 20 m).

4.1 Linear extension rate

It is known that the density banding pattern in *Porites lutea* from Phuket (Thailand) may consist of more than one pair of density bands per year due to the formation of stress bands as a result of high sedimentation rates (Brown *et al.* 1986). This became also apparent from the coral nubbins used for this study and depending on the individual coral, two or four density bands were used for detecting the annual linear extension rate. Most coral slabs displayed a clear banding pattern of two bands per year on X-radiographic and fluorescence images, which is in agreement with e.g. Knutson *et al.* (1972) and Isdale (1984). However, many pictures (especially those from the east side of Ko Miang) showed a banding pattern composed of smaller HD and LD bands, wherefore it was assumed that four bands represented one year of growth in these corals as observed by Brown *et al.* (1986) (Appendix, Fig. 17). The banding pattern of nubbins from the west side of Ko Miang was deposited in a regular and more clearly visible way compared to corals from the east, which often displayed an irregular banding pattern with more bands deposited per year. This observation could be attributed to the extreme seasonal effects of LAIW and monsoon on the west resulting in the deposition of more clearly defined patterns.

Fluorescent bands may be more advantageous for the growth measurements, as only two distinct bands per year are displayed. However, in contrast to Bösche (2012), stating that fluorescent bands were more beneficial for detecting the growth rate, the linear extension

rates in this study were primarily measured based on the X-ray images as they displayed a more distinct banding pattern. In addition, the X-radiography displays the density of the whole fragment, whereas the fluorescence technique only expresses an image of the surface of the coral slab. On many pictures, the fluorescence banding was difficult to detect and therefore it was primarily used to support the density banding pattern, which was considered as being more representative for the banding of the whole fragment. As the polyps were not cut along the growth direction on some slabs, this may have had an impact on both techniques being responsible for the difference between X-ray and fluorescence bands observed on some slabs.

The values of the linear extension rate investigated in this study (6.5-12.3 mm/yr) are consistent with observations by Lough & Barnes (1990) who state that linear extension rates of massive corals appear to range from 5 to 15 mm/yr. However, they are remarkably lower than stated by Scoffin *et al*. (1992) for *P. lutea* from the Phuket Region (10-30 mm/yr) and even for corals from Ko Miang Island (11.0-21.5 mm/yr). These differences may be attributed to the fact that corals in this study originated from 7 and 20 m depth, whereas Scoffin *et al*. (1992) collected corals at less than 1 m depth because growth rates of hermatypic corals decrease with increasing depth (Baker & Weber 1975). However, coral growth may also be limited close to the water surface due to higher wave action (Riegl 2001, Storlazzi *et al.* 2002). Higher growth rates in the Phuket Region can therefore be attributed to lower hydrodynamic impact at sheltered sites, whereas slightly lower rates at Ko Miang observed in this study, might be due to higher wave action at this island and reduced light availability at deeper depth. As light is the primary factor controlling coral growth on a vertical scale (Baker & Weber 1975, Muscatine 1990), diminishing light availability may be the main reason for reduced growth rates at 20 m depth compared to 7 m.

Contrary to the expectations of inversely related coral growth to LAIW-impact, no significant differences of the linear extension rates between side (W and E) and depth (7m and 20 m) were detected in this study (Fig. 6). Therefore, the first and second hypotheses were not fulfilled. These findings are in contrast to Schmidt & Richter (2013), who determined suppressed coral growth at the LAIW-exposed site (W 20 m) in comparison with the monsoon-exposed site (W 7 m) and the sheltered sites at the east. They concluded an inverse relationship between coral growth and LAIW. Roder *et al.* (2010, 2011) agree on the statement that the west side of the Similan Islands is more affected by LAIW due to stronger daily

temperature ranges (see also Fig. 5). According to Roder *et al*. (2011), LAIW are the most important factor influencing the reefs at the Similan Islands because the lack of a reef framework at the west can be attributed to high LAIW intensity (Schmidt 2010, Schmidt *et al.* 2012).

The linear extension rates in this study also did not show a correlation with the LAIW-index despite decreasing growth rates with increasing LAIW intensity (Fig. 11, Tab. 5). As has been expected, linear extension rates were lower at 20 m depth compared to 7 m (Fig. 6). Slightly lower growth rates at 20 m depth can be attributed to the higher impact of LAIW at deeper depth (Schmidt & Richter 2013). However, it was expected that the abrupt changes in temperature and nutrient concentration due to LAIW would significantly reduce coral growth at the exposed sites.

The fact that most coral nubbins only displayed a banding pattern of one to two years provides a possible explanation for the unexpected results of this study. Therefore, only a short growth period has been considered for this study, which might not be representative. Nevertheless, Bösche (2012) examined fragments with more bands, but also did not determine differences in the linear extension rate of *P. lutea* between study sites due to the impact of LAIW. In addition, Scoffin *et al.* (1992) also only measured linear extension rates for two years. Another possible interpretation for the deviating results in comparison with Schmidt & Richter (2013) could be the circumstance that different methods have been used in order to determine the growth rates of *P. lutea*. Schmidt & Richter (2013) determined growth rates gravimetrically (i.e. by using the buoyant weighing technique) and compared growth rates before and after the transplant experiment. In contrast, growth rates were determined in this study by measuring the annual density and fluorescent bands of the coral skeletons. This is in accordance with Brown *et al.* (1986), Scoffin *et al*. (1992) and Bösche (2012), whose results correspond with the findings of the present study. Contrasting results with regard to the impact of LAIW on linear extension rates in several studies can therefore be attributed to the two different methods used. In addition, the sample size of 11 to 15 nubbins per study site may have led to the large variance in the data and a larger sample size might have resulted in clearer results.

The monsoon seemed not to have an effect on linear extension rates of *P. lutea* at shallow depths because growth rates at W 7 m were not significantly lower compared to E 7 m. This

agrees with findings of Schmidt & Richter (2013), who state that the impact of the monsoon did not limit linear extension rates by higher surface swell but might have a positive effect on coral growth due to high wave action counteracting stressful sedimentation on corals. On the contrary, Brown *et al*. (1986) and Scoffin *et al.* (1992) observed significantly lower linear extension rates due to higher hydraulic energies and concluded that linear extension is negatively related to wave action due to monsoon exposure. In addition, Smith *et al.* (2007) also observed lower growth rates of *P. lobata* at a fore reef with higher wave energy.

4.2 Skeletal density and porosity

During the implementation of the buoyant weighing method, it is unlikely that air was trapped in the skeletal voids because the coral sticks were soaked in water for several days. In addition, water was pumped through the skeletons repeatedly. Therefore, it is unlikely that the measurement of the skeletal matrix volume for the calculation of micro-density and porosity was biased by incomplete filling of the skeletal voids. Otherwise, this would have led to overestimation of the matrix volume resulting in an underestimation of micro-density. The scatter plot of skeletal bulk density against porosity displays a correlation coefficient of $R^2 = 0.537$ (Appendix, Fig. 16). This illustrates that both parameters are inversely correlated as has been expected according to Bucher *et al.* (1998). This inverse relationship is also apparent in the results and leads to the conclusion that the buoyant weighing technique provided reasonable results (Fig. 7 and 9, Bucher *et al.* 1998).

The weight of the paraffin wax, which has been added to the coral sticks to prevent water to re-enter the skeletal voids, is not known. Therefore, this additional material might have biased the calculation of the total enclosed volume and the values of the skeletal bulk density and porosity accordingly. Even though it was paid attention to only add a very thin wax coating to the sticks, they exhibited different lengths and therefore variable amounts of wax were added to the sticks. For more precise calculations, the wax coating would have to be removed from the sticks in order to weight the wax used for each stick separately. This value would then have to be subtracted from the measured dry and buoyant weight of the waxed coral skeletons. However, none of the studies that developed and used this method, mention this issue and only state that a thin layer of wax barely influences the measurements (Oliver *et al.* 1983, Risk & Sammarco 1991, Bucher *et al.* 1998, Smith *et al.* 2007,

Manzello 2010). The optimum temperature of the paraffin wax was adjusted in order to form only a thin layer of wax because a thicker layer would have significantly affected the total enclosed volume (Bucher *et al.* 1998).

The values of skeletal bulk density determined by this study (1.1-1.7 g/cm^3) are similar to those observed by Scoffin *et al.* (1992) from Ko Miang (1.3-1.6 g/cm^3). The skeletal bulk density of *P. lutea* revealed significant differences between the two sides of Ko Miang with higher values at the exposed west side of the island (Fig. 7, Tab. 1). This finding supports the hypothesis that the impact of LAIW and monsoon results in greater skeletal densities at the west side. However, greater skeletal densities at shallow depth with significantly greater values at W 7 m compared to E 7 m lead to the assumption that the impact of the monsoon is primarily responsible for the higher densities. These findings are in agreement with Brown *et al.* (1986), Scoffin *et al.* (1992) and Smith *et al.* (2007), who discovered greater skeletal densities of corals growing at wave-exposed sites compared to sheltered sites.

No correlation of the skeletal bulk density with the LAIW-index has been discovered (Fig. 12, Tab. 5), which also supports the assumption that the monsoon primarily influences the skeletal density. This finding is in contrast to Wall *et al.* (2012), who discovered an impact of both LAIW and monsoon on corals at the west side of the Similan Islands. Higher skeletal densities observed at the exposed west side of Ko Miang by Bösche (2012) were attributed to the impact of the LAIW, even though the correlation of the skeletal density with the LAIW-index failed to be significant, which is in agreement with the present study. Corals that are exposed to higher hydraulic energies at the water surface probably deposit more calcium carbonate in order to increase the stability of their skeleton. According to Smith *et al.* (2007), increasing bulk density as a result of higher mechanical impact may occur in order to reduce the tendency of breakage of the coral.

The results for the porosity of *P. lutea* also provide support for this hypothesis, as findings are inversely related to the results of the skeletal bulk density as has been expected (Bucher *et al.* 1998). Nubbins collected at the sheltered E revealed significantly higher porosity values than corals from the exposed W, resulting in lower skeletal bulk densities at the E and higher densities at the W respectively (Fig. 9, Tab. 3). In addition, higher values were determined at E 7 m compared to E 20 m and W 7 m, which also supports the assumption that the skeletal density at W 7 m is mainly influenced by monsoon exposure. Higher porosity of

the coral skeletons were observed with lower impact of LAIW but no significant correlation was determined (Fig. 14, Tab. 5).

The micro-density revealed significantly higher values at 7 m compared to 20 m with higher values at E 7 m compared to E 20 m and W 7 m (Fig. 8, Tab. 2). Higher micro-density values at shallow compared to deeper depth reinforce the impact of the monsoon on the density of the skeleton of *P. lutea*. Bucher *et al.* (1998) discovered no significant differences in the micro-density due to wave exposure which would explain why values of micro-density observed in this study were not higher at W 7 m as for the skeletal bulk density. However, this is no explanation for significantly higher micro-densities at E 7 m.

4.3 Calcification rate

The calcification rate of *P. lutea* did not show statistically significant differences between the four study sites (Fig. 10). These results correspond with findings of Scoffin *et al.* (1992) who discovered no apparent relationship between calcification rate and hydrodynamic conditions. However, Schmidt (2010) discovered significantly lower calcification rates at the exposed W compared to the sheltered E with significantly higher accretion rates at E 7 m than at E 20 m and W 7 m.

It is not surprising that the calcification rates observed in this study do not display significant differences, as the calcification rate is controlled by variations in the linear extension rate as a result of a positive correlation between linear extension and calcification rate (Scoffin *et al.* 1992, Lough & Barnes 2000, Smith *et al.* 2007). Since skeletal bulk density and growth rates of *Porites* are inversely correlated (Scoffin *et al.* 1992, Lough & Barnes 2000), observed higher bulk densities at the west side do not necessarily lead to higher calcification rates. In addition, due to higher light availability near the water surface leading to light-enhanced calcification in zooxanthellate scleractinian corals (Gattuso *et al.* 1999), higher solar irradiance may be an explanation for the supposed higher values observed in this study at shallow depth (Lough & Barnes 2000). Another possible explanation are enhanced metabolic and calcification rates due to higher water motion at shallow depth (Dennison & Barnes 1988), which may also have been beneficial for the corals because of the prevention of stressful sedimentation on the corals' surface (Schmidt & Richter 2013).

As calcification is dependent on a high aragonite saturation state and LAIW suppress pH values at the west of the Similan Islands, significantly lower calcification rates at W 20 m were expected. However, the coupled influence of linear extension rate and skeletal bulk density on calcification rates may conceal this effect. Since no correlation of calcification rate with the LAIW-index was found, other factors, such as light availability or water motion, are likely to affect calcification rates of *P. lutea* more strongly than reduced aragonite saturation due to internal waves.

The calcification rates determined in this study (0.92-2.01 g/cm^2) were much lower in comparison to those observed by Scoffin *et al.* (1992) from Ko Miang (1.74-2.98 g/cm^2). This may be attributed to lower linear extension rates detected in this study compared to Scoffin *et al.* (1992).

4.4 Correlation with LAIW-index

The scatter plots do not illustrate a significant correlation of the parameters linear extension rate, skeletal density and calcification rate with the LAIW-index (Fig. 11-15, Tab. 5). Other environmental factors such as variations in light availability and wave action at the surface instead of differences in temperature, seem to primarily influence the parameters at shallow and deep study sites. Consequently, other factors than internal waves seem to be more important for affecting growth and skeletal density of *P. lutea*. In addition, all graphs display large standard deviations, leading to the assumption that this high variability of the data prohibits a clear trend and correlation with temperature variations.

5 Conclusion and prospects

The impact of the monsoon was apparent in the skeletal bulk density of the massive scleractinian coral *Porites lutea* from the central Similan island Ko Miang, but not in linear extension rate and calcification rate. This was especially evident for shallow depth leading to the conclusion that the skeletal density is more influenced by the monsoon than by LAIW. As the results of the linear extension rate and calcification rate of *P. lutea* did not reveal significant differences between side and depth, no influence by LAIW or monsoon has been detected. In addition, none of the three skeletal parameters showed a correlation with the LAIW-index, reinforcing the aforementioned finding.

The impact of LAIW and monsoon will have to be determined further in future studies in order to investigate an undisputed statement about their effect on coral growth and reef development. This is especially necessary for the effect on linear extension rates because opposing findings exist on the effect of LAIW on coral growth rates. To further investigate the effect of LAIW and monsoon on corals separately, organisms should be examined at study sites that are only influenced by one of the two environmental phenomena. This would allow to exclude the effect of the other phenomenon and draw more precise conclusions. In order to generalise the effect of LAIW and monsoon on coral growth, other coral species apart from the model organism *P. lutea* should also be included in studies. It is furthermore necessary to detect a standardised technique to determine the effect of LAIW and monsoon on coral growth in future studies, as it has been shown that different methods for the measurement of growth rates resulted in contradicting findings.

6 Literature

Achituv Y & Dubinsky Z (1990) Evolution and Zoogeography of Coral Reefs, in: Dubinsky Z (ed.) Ecosystems of the World: Coral Reefs. Elsevier Science Publishers, Amsterdam, pp. 1-9.

Baker PA & Weber JN (1975) Coral growth rate: variation with depth. Earth and Planetary Science Letters, 27(1): 57-61.

Barnes DJ & Devereux MJ (1988) Variations in skeletal architecture associated with density banding in the hard coral *Porites*. Journal of Experimental Marine Biology and Ecology, 121(1): 37-54.

Barnes DJ & Lough JM (1993) On the nature and causes of density banding in massive coral skeletons. Journal of Experimental Marine Biology and Ecology, 167(1): 91-108.

Barnes DJ & Taylor RB (2001) On the nature and causes of luminescent lines and bands in coral skeletons. Coral Reefs, 19(3): 221-230.

Birkeland C (1988) Geographic comparisons of coral-reef community processes. Proc. 6th Int. Coral Reef Symp.

Boto K & Isdale P (1985) Fluorescent bands in massive corals result from terrestrial fulvic acid inputs to nearshore zone. Nature, 315(6018): 396-397.

Brown BE (2007) Coral reefs of the Andaman Sea – an integrated perspective. Oceanography and marine biology: an annual review, 45: 173-194.

Brown B, Le Tissier M, Howard LS, Charuchinda M & Jackson JA (1986) Asynchronous deposition of dense skeletal bands in *Porites lutea*. Marine Biology, 93(1): 83-89.

Bucher DJ, Harriott VJ & Roberts LG (1998) Skeletal micro-density, porosity and bulk density of acroporid corals. Journal of Experimental Marine Biology and Ecology, 228(1): 117-136.

Buddemeier RW & Kinzie RA (1976) Coral growth. Oceanography and Marine Biology Annual Review, 14: 183-225.

Buddemeier RW, Maragos JE & Knutson DW (1974) Radiographic studies of reef coral exoskeletons: rates and patterns of coral growth. Journal of Experimental Marine Biology and Ecology, 14(2): 179-199.

Bösche K (2012) Effect of seasonal large amplitude internal waves (LAIW) on annual coral growth and skeletal density of the coral *Porites lutea*. Bachelor thesis, University of Bremen.

Davies PS (1989) Short-term growth measurements of corals using an accurate buoyant weighing technique. Marine Biology, 101(3): 389-395.

Dennison WC & Barnes DJ (1988) Effect of water motion on coral photosynthesis and calcification. Journal of Experimental Marine Biology and Ecology, 115(1): 67-77.

Dodge RE & Vaisnys JR (1975) Hermatypic coral growth banding as environmental recorder. Nature, 258: 706-708.

Dodge RE, Aller RC & Thomson J (1974) Coral growth related to resuspension of bottom sediments. Nature, 247: 574 – 577.

Gattuso JP, Allemand D & Frankignoulle M (1999) Photosynthesis and calcification at cellular, organismal and community levels in coral reefs: a review on interactions and control by carbonate chemistry. American Zoologist, 39(1): 160-183.

Gattuso JP, Frankignoulle M, Bourge I, Romaine S & Buddemeier RW (1998) Effect of calcium carbonate saturation of seawater on coral calcification. Global and Planetary Change, 18(1): 37-46.

Highsmith RC (1979) Coral growth rates and environmental control of density banding. Journal of Experimental Marine Biology and Ecology, 37(2): 105-125.

Hudson JH, Shinn EA, Halley RB & Lidz B (1976) Sclerochronology: a tool for interpreting past environments. Geology, 4(6): 361-364.

Isdale P (1984) Fluorescent bands in massive corals record centuries of coastal rainfall. Nature, 310(5978): 578-579.

Jackson CR (2004). An atlas of internal solitary-like waves and their properties. 2nd edition. Office of Naval Research, Global Ocean Associates, Alexandria, VA, USA

Klein R, Loya Y, Gvirtzman G, Isdale PJ & Susic M (1990) Seasonal rainfall in the Sinai Desert during the late Quaternary inferred from fluorescent bands in fossil corals. Nature, 345(6271): 145-147.

Kleypas JA, McManus JW & Meñez LAB (1999a) Environmental limits to coral reef development: where do we draw the line? American Zoologist, 39(1): 146-159.

Kleypas JA, Buddemeier RW, Archer D, Gattuso JP, Langdon C & Opdyke BN (1999b) Geochemical Consequences of Increased Atmospheric Carbon Dioxide on Coral Reefs. Science, 284(5411): 118-120.

Knutson DW, Buddemeier RW & Smith SV (1972) Coral chronometers: seasonal growth bands in reef corals. Science, 177(4045): 270-272.

Leichter JJ & Miller SL (1999) Predicting high-frequency upwelling: Spatial and temporal patterns of temperature anomalies on a Florida coral reef. Continental Shelf Research, 19(7): 911-928.

Leichter JJ, Deane GB & Stokes MD (2005) Spatial and temporal variability of internal wave forcing on a coral reef. Journal of Physical Oceanography, 35(11): 1945-1962.

Leichter JJ, Stewart HL & Miller SL (2003) Episodic nutrient transport to Florida coral reefs. Limnology and Oceanography, 48(4): 1394-1407.

Lough JM & Barnes DJ (1990) Intra-annual timing of density band formation of *Porites* coral from the central Great Barrier Reef. Journal of Experimental Marine Biology and Ecology, 135(1): 35-57.

Lough JM & Barnes DJ (2000) Environmental controls on growth of the massive coral *Porites*. Journal of Experimental Marine Biology and Ecology, 245(2): 225-243.

Manzello DP (2010) Coral growth with thermal stress and ocean acidification: lessons from the eastern tropical Pacific. Coral Reefs, 29(3): 749-758.

Muller-Parker G & D'Elia CF (1997) Interactions Between Corals and Their Symbiotic Algae, in: Birkeland C (ed.) Life and Death of Coral Reefs. Springer Science & Business Media, International Thomson Publishing, New York, pp. 96-113.

Muscatine L (1990) The Role of Symbiotic Algae in Carbon and Energy Flux in Reef Corals, in: Dubinsky Z (ed.) Ecosystems of the World: Coral Reefs. Elsevier Science Publishers, Amsterdam, pp. 75-87.

Nie B, Chen T, Liang M, Wang Y, Zhong J, & Zhu Y (1997) Relationship between coral growth rate and sea surface temperature in the northern part of South China Sea during the past 100 a. Science in China Series D: Earth Sciences, 40(2): 173-182.

Ohde S & Hossain MMM (2004) Effect of CaCO3 (aragonite) saturation state of seawater on calcification of *Porites* coral. Geochemical Journal, 38: 613-621.

Oliver JK, Chalker BE & Dunlap WC (1983) Bathymetric adaptations of reef-building corals at Davies Reef, Great Barrier Reef, Australia - I. Long-term growth responses of *Acropora formosa* (Dana 1846). Journal of Experimental Marine Biology and Ecology, 73(1): 11-35.

Osborne AR & Burch TL (1980) Internal solitons in the Andaman Sea. Science, 208(4443): 451-460.

Pearse VB & Muscatine L (1971) Role of symbiotic algae (zooxanthellae) in coral calcification. The Biological Bulletin, 141(2): 350-363.

Perry RB & Schimke GR (1965) Large-amplitude internal waves observed off the northwest coast of Sumatra. Journal of Geophysical Research, 70(10): 2319-2324.

Riegl B (2001) Inhibition of reef framework by frequent disturbance: examples from the Arabian Gulf, South Africa, and the Cayman Islands. Palaeogeography, Palaeoclimatology, Palaeoecology, 175(1): 79-101.

Riegl B & Bloomer JP (1995) Tissue damage in scleractinian and alcyonacean corals due to experimental exposure to sedimentation. Oceanography Faculty Proceedings, Presentations, Speeches, Lectures. Paper 114.

Risk MJ & Sammarco PW (1991) Cross-shelf trends in skeletal density of the massive coral *Porites lobata* from the Great Barrier Reef. Marine Ecology Progress Series, Oldendorf, 69(1): 195-200.

Roder C, Fillinger L, Jantzen C, Schmidt GM, Khokiattiwong S & Richter C (2010) Trophic response of corals to large amplitude internal waves. Marine Ecology Progress Series, 412: 113-128.

Roder C, Jantzen C, Schmidt GM, Kattner G, Phongsuwan N & Richter C (2011) Metabolic plasticity of the corals *Porites lutea* and *Diploastrea heliopora* exposed to large amplitude internal waves. Coral Reefs, 30(1): 57-69.

Schmidt GM (2010) Corals & Waves Calcification and bioerosion in Large Amplitude Internal Wave (LAIW) affected coral reefs. PhD-Thesis, University of Bremen.

Schmidt GM & Richter C (2013) Coral growth and bioerosion of *Porites lutea* in response to large amplitude internal waves. PLoS ONE, 8(12): 73236. doi: 10.1371/journal.pone.0073236.

Schmidt GM, Phongsuwan N, Jantzen C, Roder C, Khokiattiwong S & Richter C (2012) Coral community composition and reef development at the Similan Islands, Andaman Sea, in response to strong environmental variations. Marine Ecology Progress Series, 456: 113-126.

Scoffin TP, Tudhope AW & Brown BE (1989) Fluorescent and skeletal density banding in *Porites lutea* from Papua New Guinea and Indonesia. Coral Reefs, 7(4): 169-178.

Scoffin TP, Tudhope AW, Brown BE, Chansang H & Cheeney RF (1992) Patterns and possible environmental controls of skeletogenesis of *Porites lutea*, South Thailand. Coral Reefs, 11(1): 1-11.

Smith SV & Buddemeier RW (1992) Global Change and Coral Reef Ecosystems. Annual Review of Ecology and Systematics, 23: 89-118.

Smith LW, Barshis D & Birkeland C (2007) Phenotypic plasticity for skeletal growth, density and calcification of *Porites lobata* in response to habitat type. Coral Reefs, 26(3): 559-567.

Stoddart DR (1973) Coral Reefs of the Indian Ocean, in: Jones OA & Endean R (eds.) Biology and Geology of Coral Reefs – Geology I. Academic Press, New York, pp. 51-92.

Storlazzi CD, Field ME, Dykes JD, Jokiel PL & Brown E (2002) Wave control on reef morphology and coral distribution: Molokai, Hawaii, in: WAVES 2001 Conference Proceedings (Vol. 1), pp. 784-793.

Susic M, Boto K & Isdale P (1991) Fluorescent humic acid bands in coral skeletons originate from terrestrial runoff. Marine chemistry, 33(1): 91-104.

Tanzil JTI, Brown BE, Tudhope AW & Dunne RP (2009) Decline in skeletal growth of the coral *Porites lutea* from the Andaman Sea, South Thailand between 1984 and 2005. Coral Reefs, 28(2): 519-528.

Tilton LW & Taylor JK (1937) Accurate representation of the refractivity and density of distilled water as a function of temperature. Journal of Research of the National Bureau of Standards, 2(20): 205-214.

Tudhope AW, Lea DW, Shimmield GB, Chilcott CP & Head S (1996) Monsoon climate and Arabian Sea coastal upwelling recorded in massive corals from southern Oman. Palaios, 347-361.

Vlasenko V & Stashchuk N (2007) Three-dimensional shoaling of large-amplitude internal waves. Journal of Geophysical Research, 112. doi: 10.1029/2007JC004107.

Wall M, Schmidt GM, Janjang P, Khokiattiwong S & Richter C (2012) Differential impact of monsoon and large amplitude internal waves on coral reef development in the Andaman Sea. PloS ONE, 7(11): e50207. doi: 10.1371/journal.pone.0050207.

7 Appendix

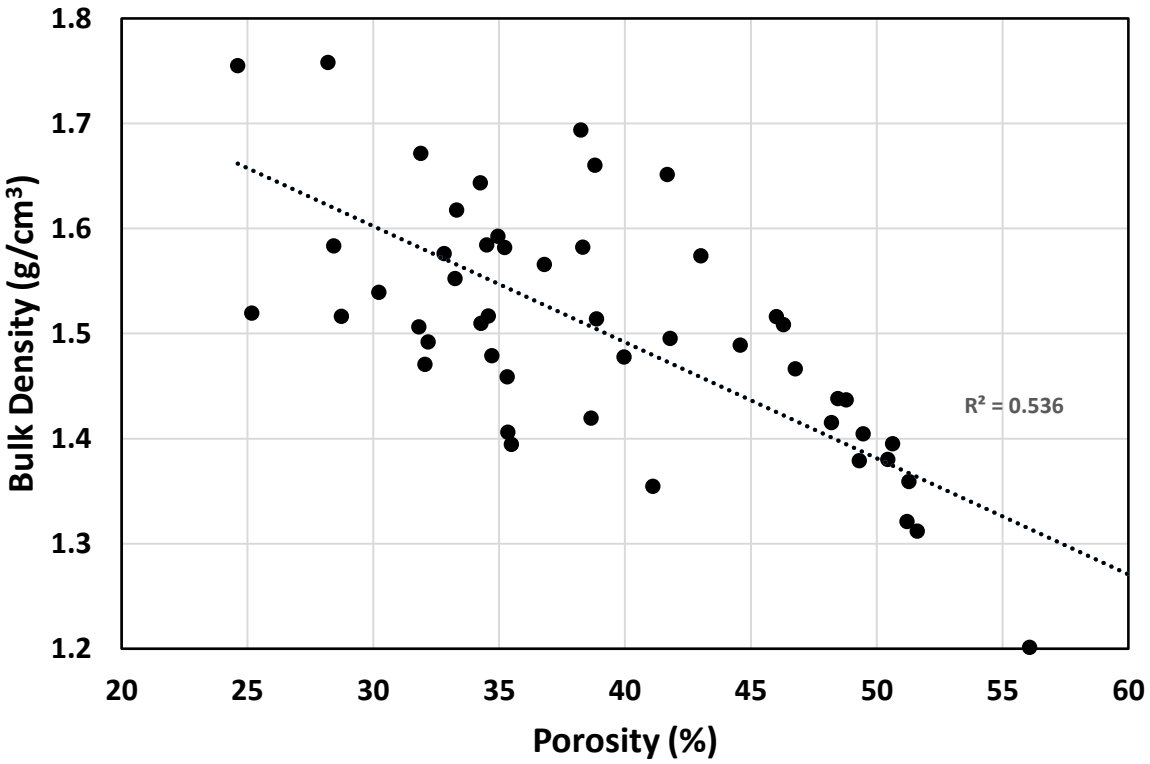

Figure 16. Scatter plot of skeletal bulk density (g/cm^3) against porosity (%) of *Porites lutea* collected at the central Similan island Ko Miang (correlation coefficient of regression line r^2 = 0.536).

Figure 17. Combined X-radiograph and fluorescence images of *Porites lutea* nubbins collected at Ko Miang Island, Similan Islands. All 50 combined pictures used to determine the annual linear growth rate are displayed (main picture). For each picture, the X-radiograph cut along three individual polyps close to the major growth axis is also shown (three small pictures). Yellow marks represent transition points between two bands. Scale represents 10 mm. For each coral nubbin, the results of linear extension rate (LER, mm/yr), skeletal bulk density (SBD, g/cm^3), micro-density (MD, g/cm^3), porosity (P, %), and calcification rate (CR, g/cm^2) are also displayed. Study sites: Fragments 01-11 = E 7m, fragments 12-27 = E 20 m, fragments 28-41 = W 20 m, fragments 43-53 = W 7 m.

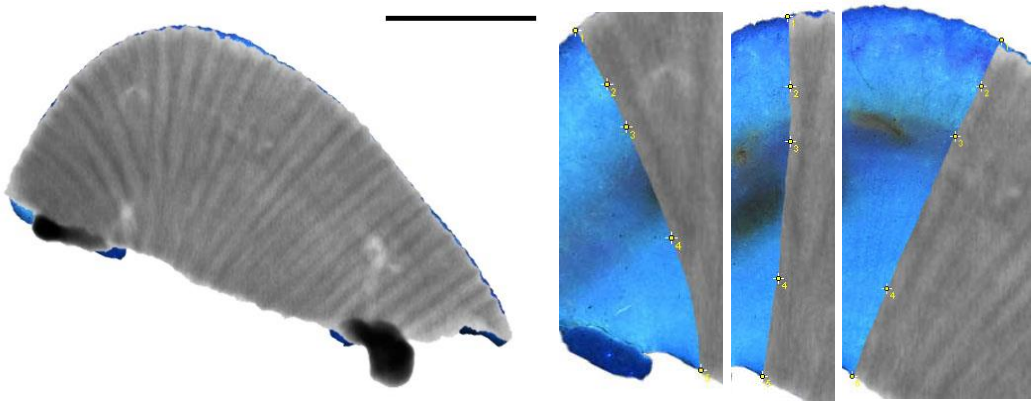

Fragment 01
LER: 7.863
SBD: 1.437
MD: 2.805
P: 48.780
CR: 1.130

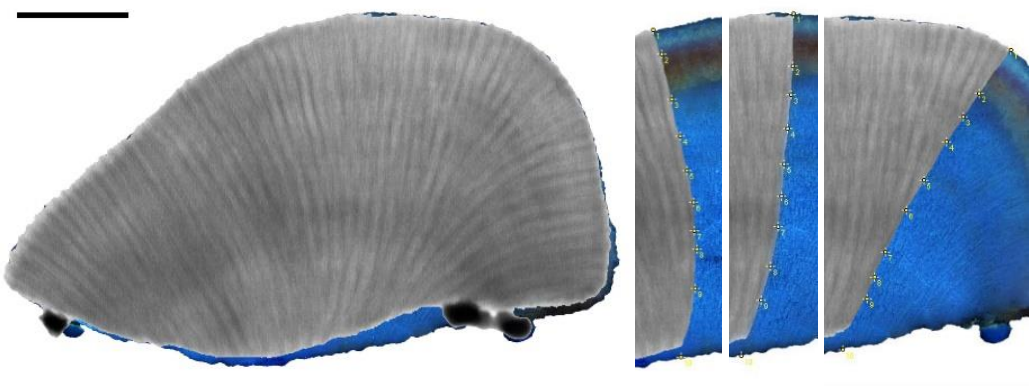

Fragment 02
LER: 12.314
SBD: 1.516
MD: 2.808
P: 46.009
CR: 1.867

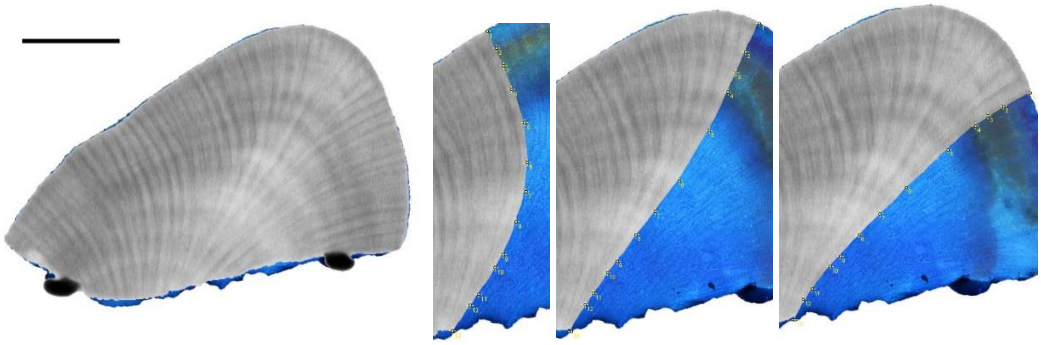

Fragment 03
LER: 10.065
SBD: 1.321
MD: 2.706
P: 51.198
CR: 1.329

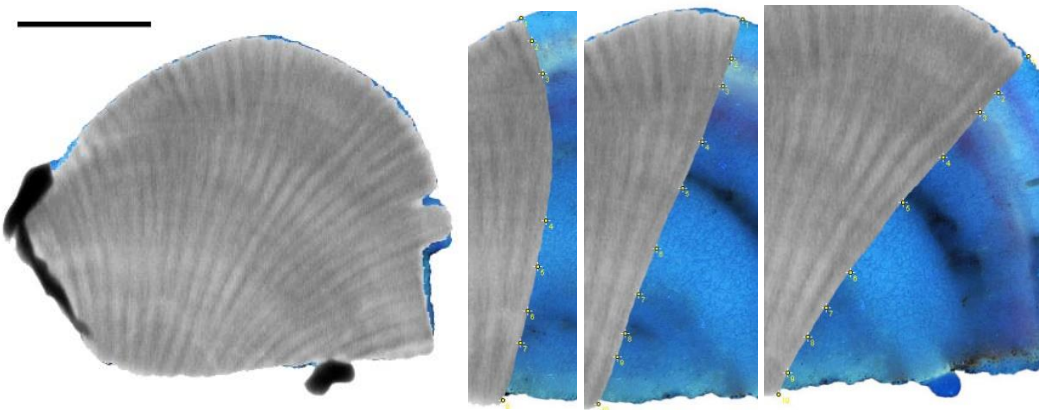

Fragment 04
LER: 11.958
SBD: 1.438
MD: 2.789
P: 48.452
CR: 1.719

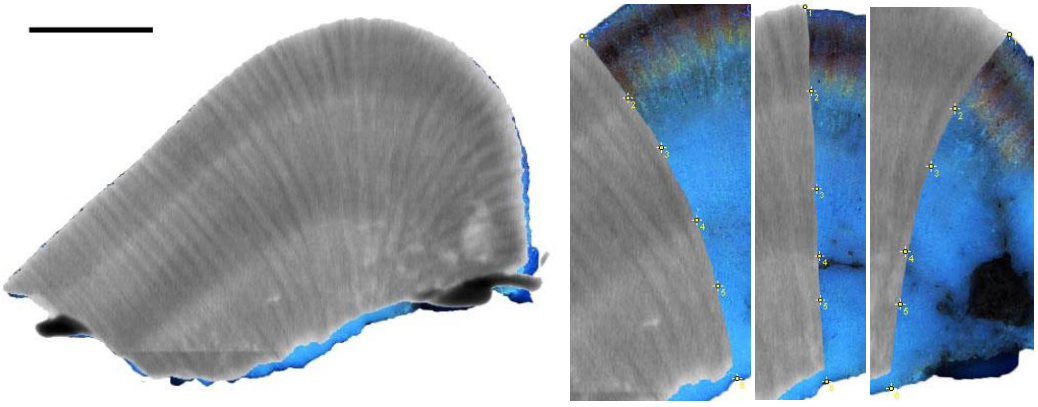

Fragment 05a
LER: 8.548
SBD: 1.644
MD: 2.499
P: 34.240
CR: 1.405

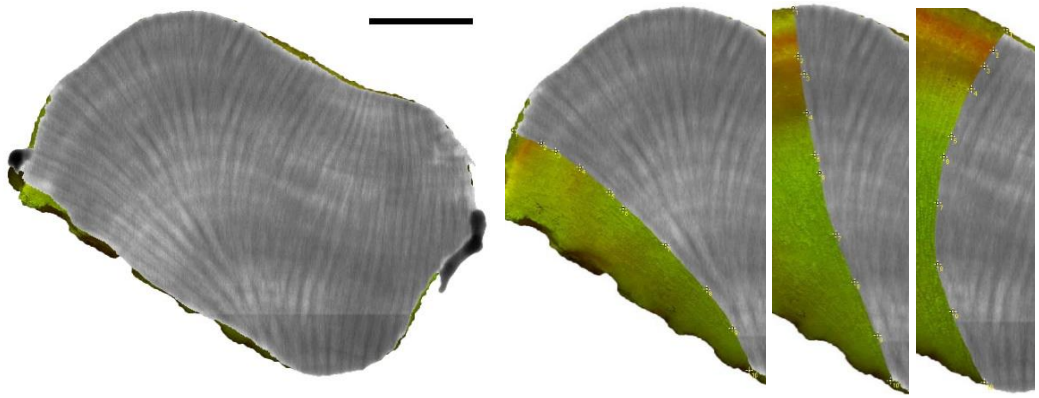

Fragment 05b
LER: 9.559
SBD: 1.404
MD: 2.778
P: 49.450
CR: 1.342

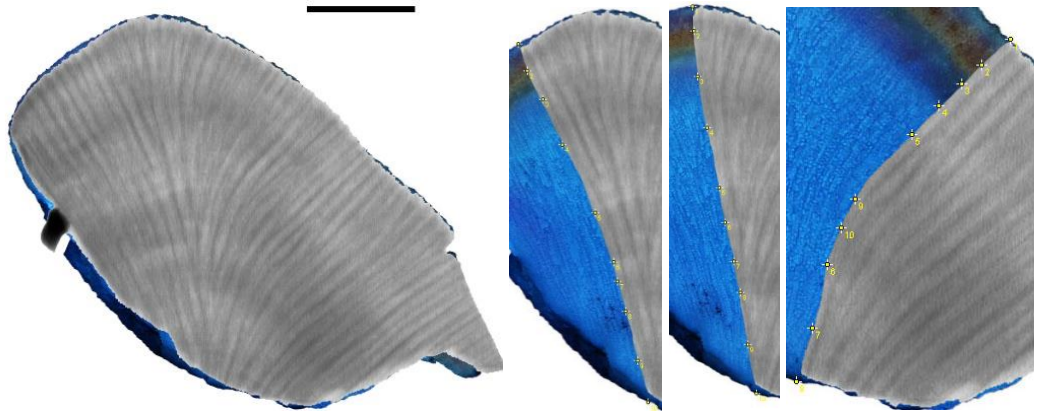

Fragment 06
LER: 8.618
SBD: 1.359
MD: 2.789
P: 51.279
CR: 1.171

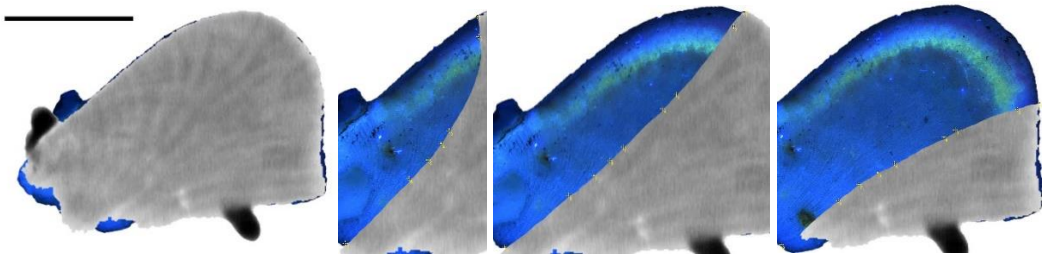

Fragment 07a
LER: 8.245
SBD: 1.477
MD: 2.461
P: 39.958
CR: 1.218

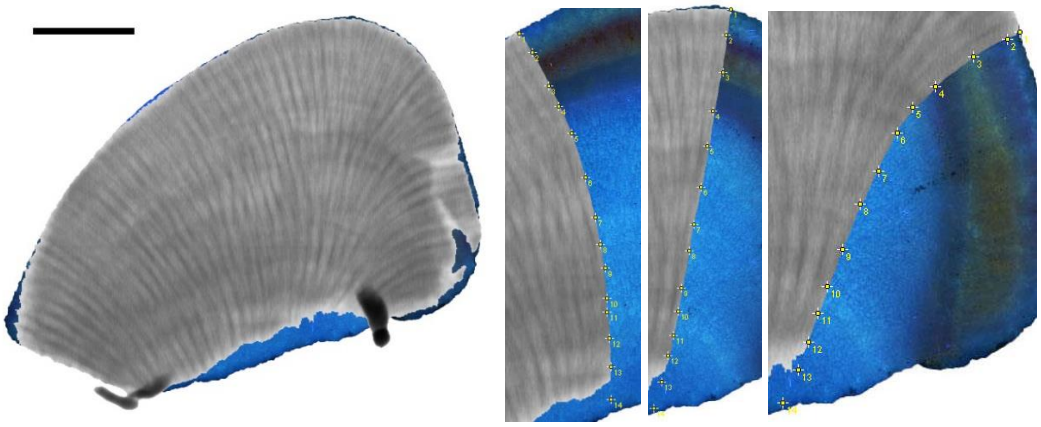

Fragment 07b
LER: 10.184
SBD: 1.380
MD: 2.784
P: 50.430
CR: 1.406

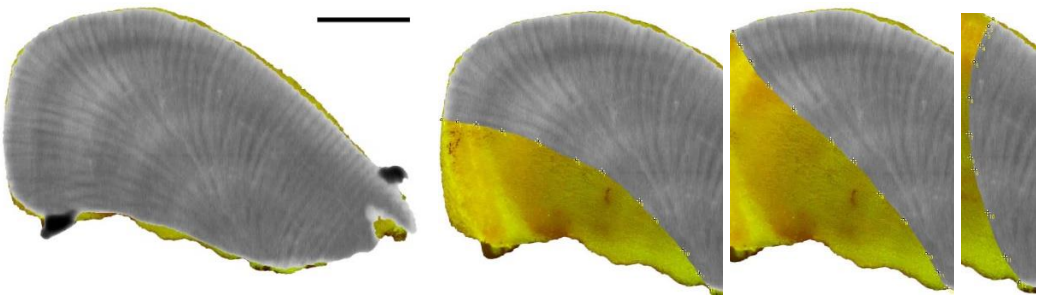

Fragment 08
LER: 11.885
SBD: 1.694
MD: 2.742
P: 38.241
CR: 2.013

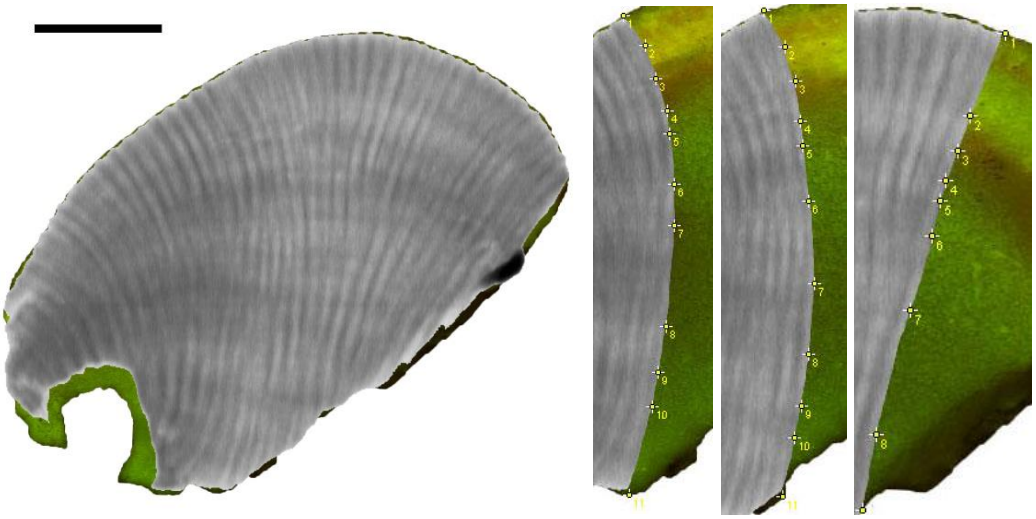

Fragment 09
LER: 10.101
SBD: 1.379
MD: 2.720
P: 49.305
CR: 1.393

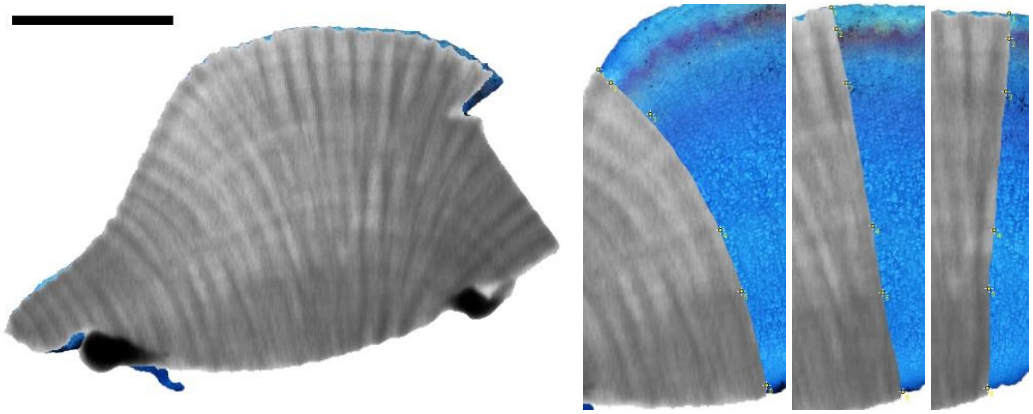

Fragment 11
LER: 9.822
SBD: 1.201
MD: 2.734
P: 56.063
CR: 1.180

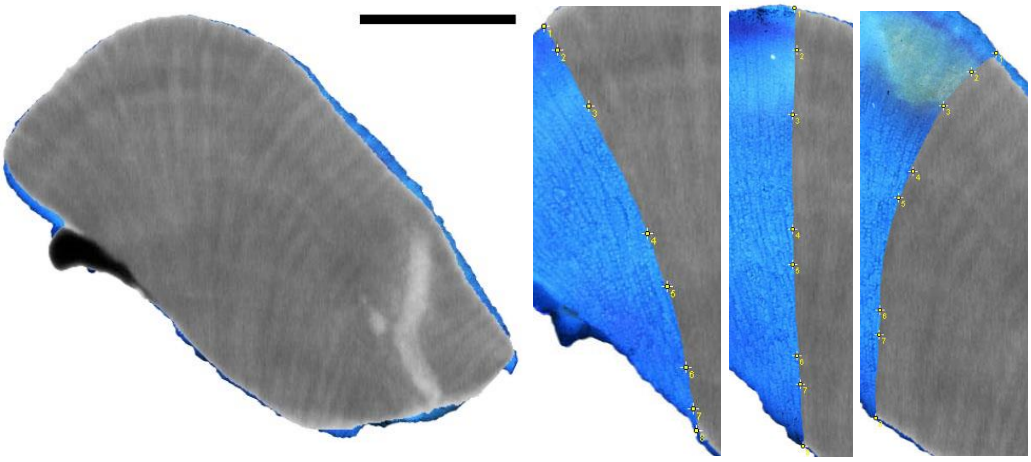

Fragment 12
LER: 7.158
SBD: 1.510
MD: 2.297
P: 34.270
CR: 1.081

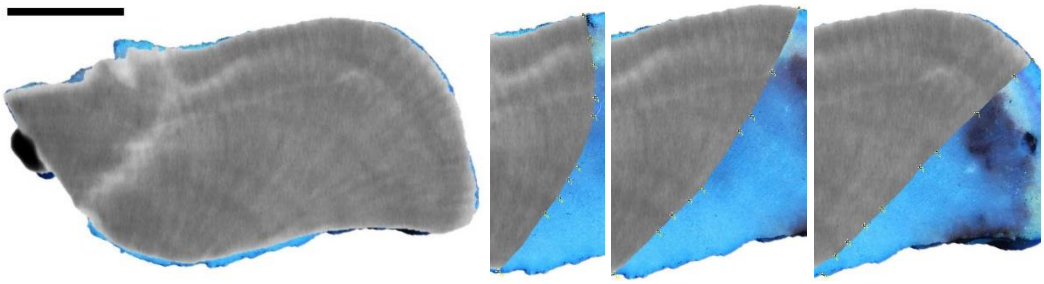

Fragment 13
LER: 8.059
SBD: 1.514
MD: 2.476
P: 38.869
CR: 1.220

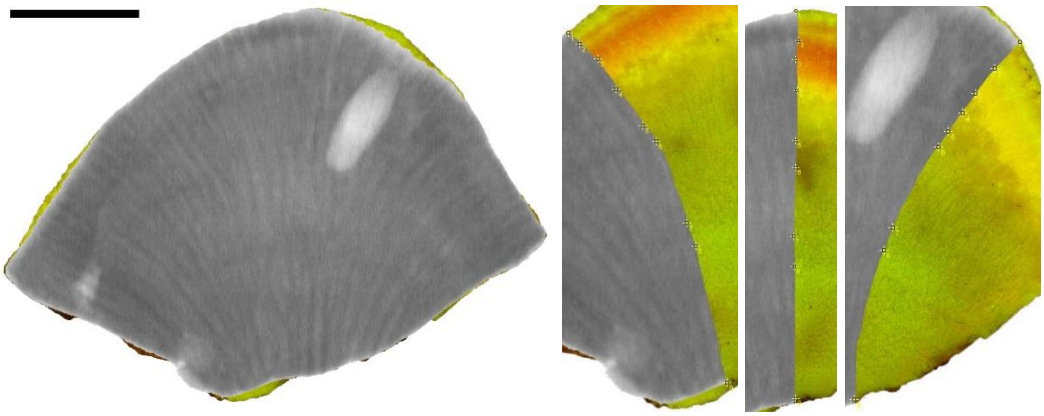

Fragment 14
LER: 7.413
SBD: 1.354
MD: 2.300
P: 41.097
CR: 1.004

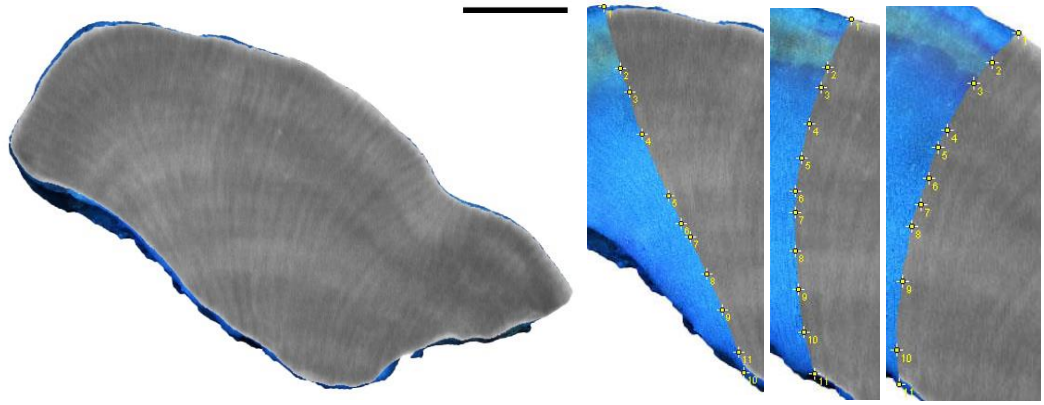

Fragment 15
LER: 11.151
SBD: 1.419
MD: 2.313
P: 38.642
CR: 1.583

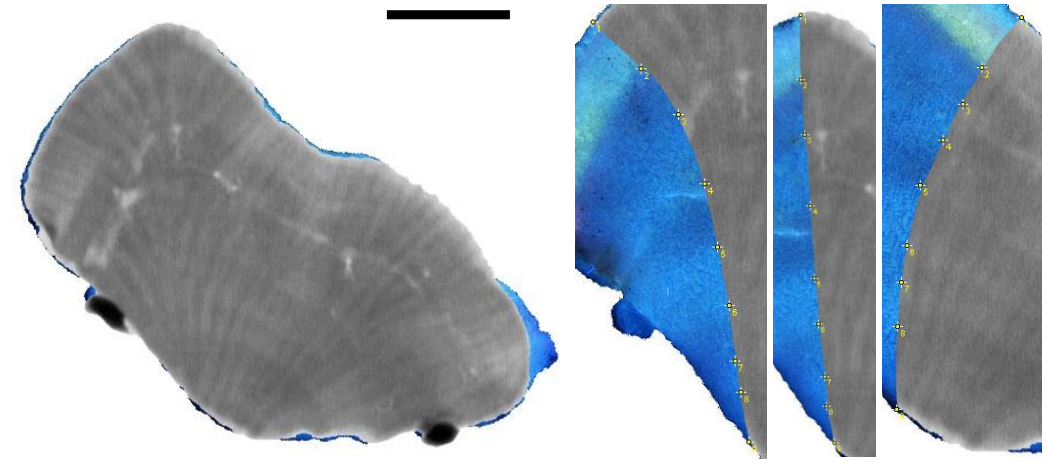

Fragment 16
LER: 6.521
SBD: 1.519
MD: 2.030
P: 25.161
CR: 0.991

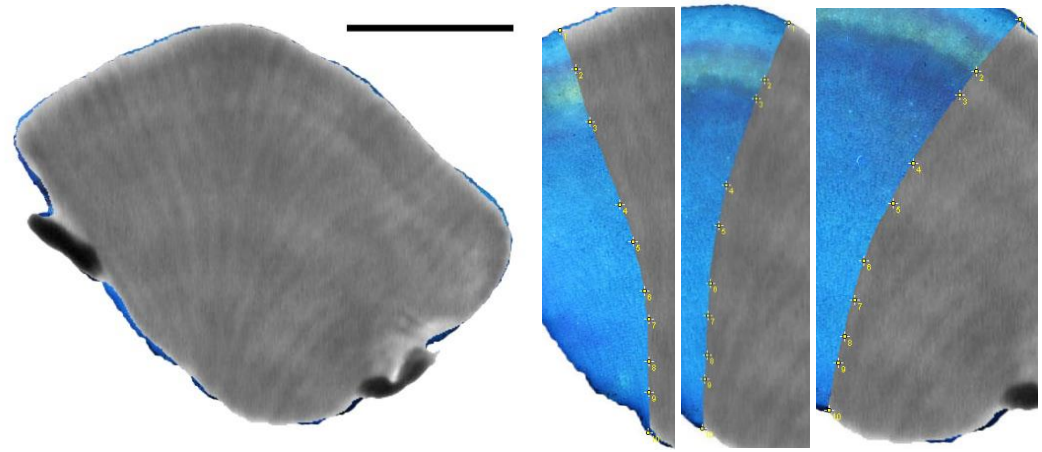

Fragment 17
LER: 9.264
SBD: 1.583
MD: 2.212
P: 28.424
CR: 1.467

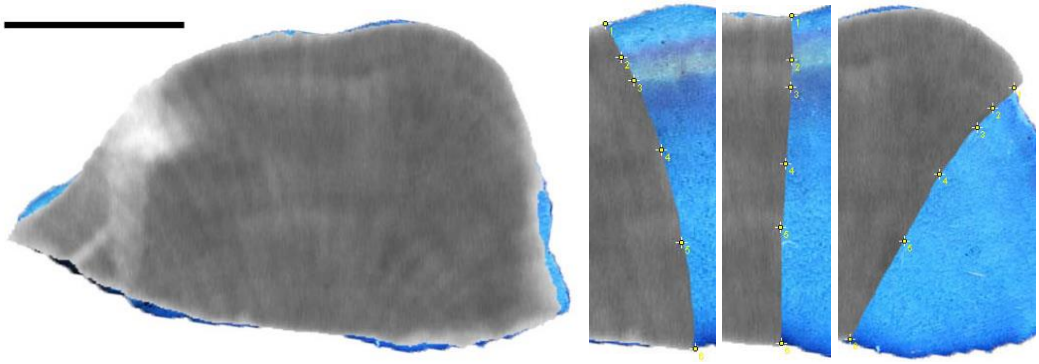

Fragment 18
LER: 11.558
SBD: 1.506
MD: 2.209
P: 31.808
CR: 1.741

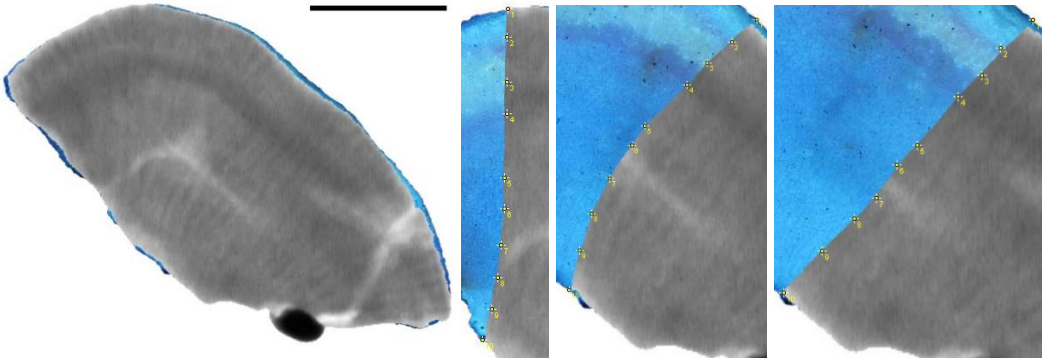

Fragment 19
LER: 7.483
SBD: 1.582
MD: 2.442
P: 35.215
CR: 1.184

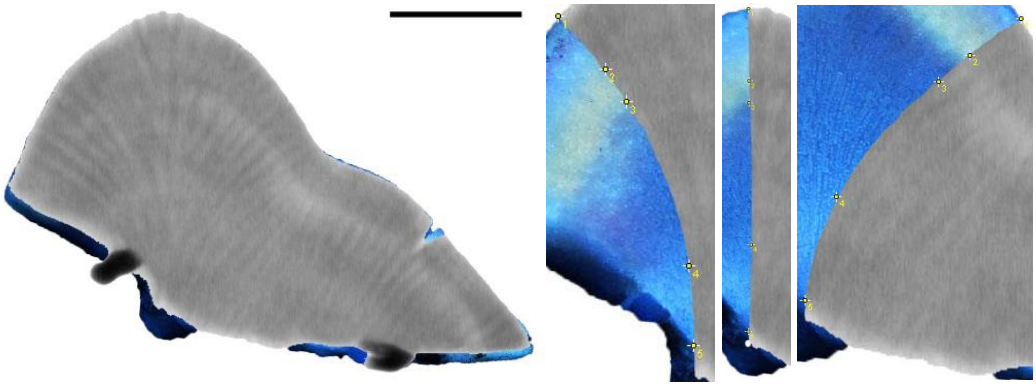

Fragment 21
LER: 10.316
SBD: 1.471
MD: 2.164
P: 32.051
CR: 1.517

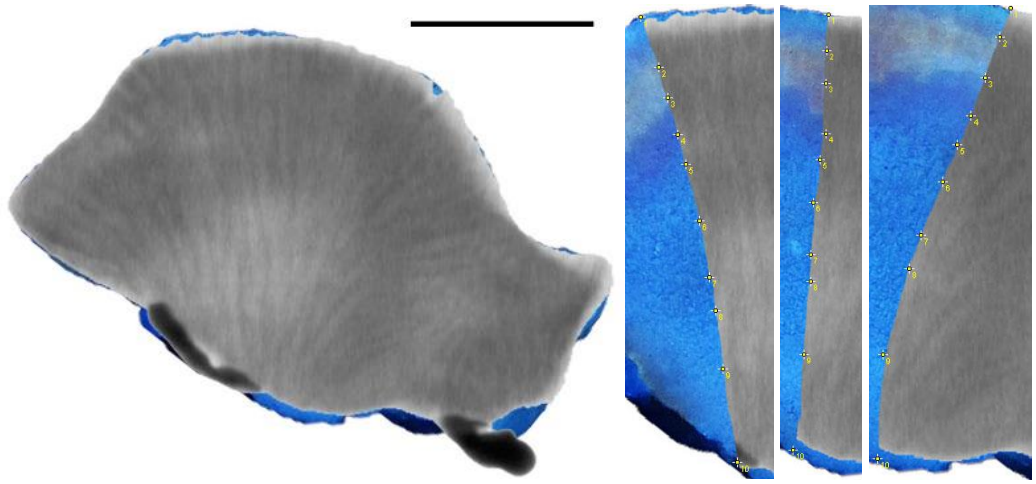

Fragment 22
LER: 7.281
SBD: 1.479
MD: 2.265
P: 34.702
CR: 1.077

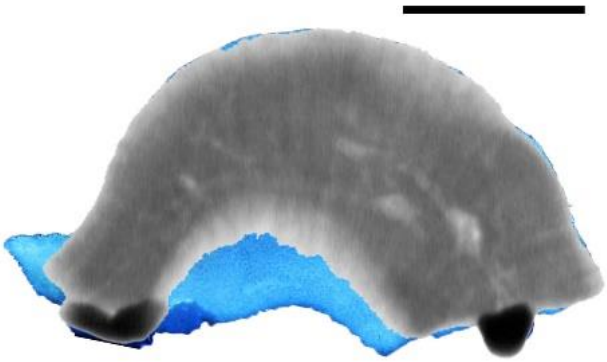

Fragment 23
LER: -
SBD: 1.582
MD: 2.565
P: 38.309
CR: -

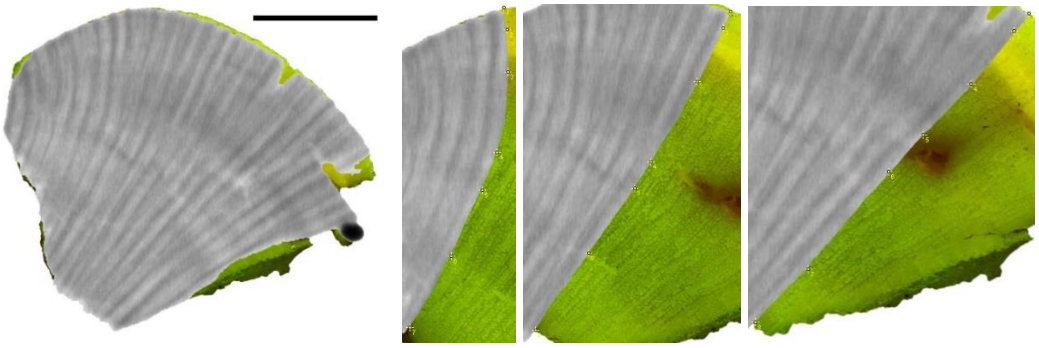

Fragment 24
LER: 8.362
SBD: 1.101
MD: 2.796
P: 60.629
CR: 0.920

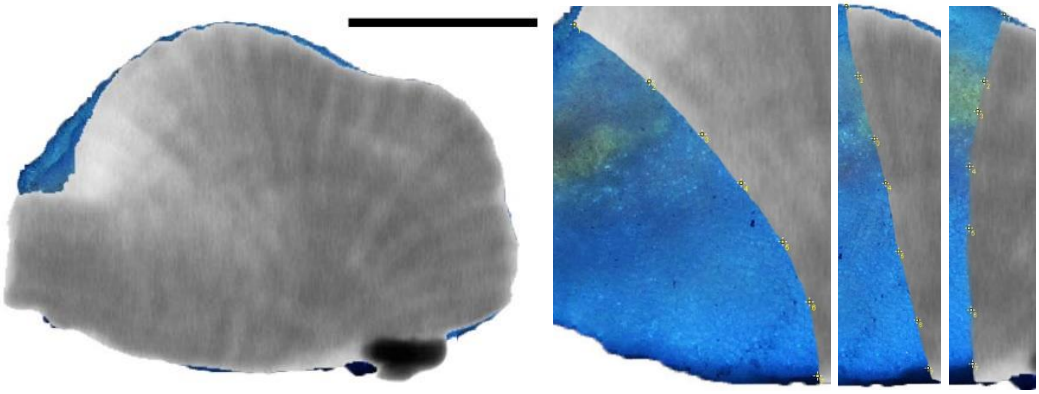

Fragment 25
LER: 11.040
SBD: 1.492
MD: 2.200
P: 32.176
CR: 1.647

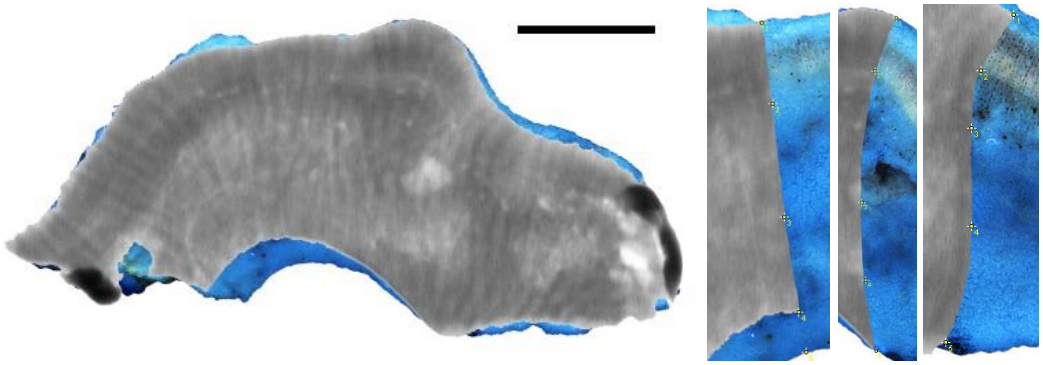

Fragment 26
LER: 10.366
SBD: 1.574
MD: 2.762
P: 43.011
CR: 1.631

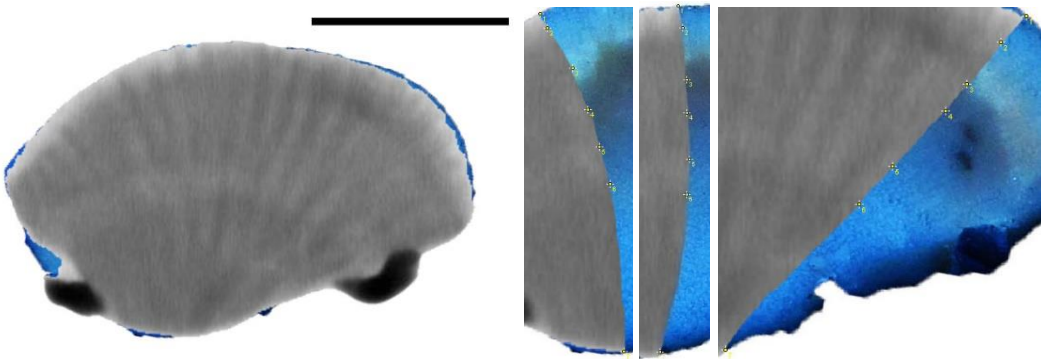

Fragment 27
LER: 7.100
SBD: 1.489
MD: 2.686
P: 44.570
CR: 1.057

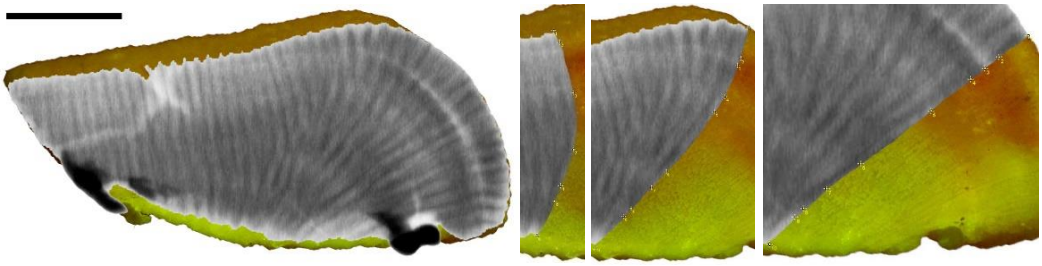

Fragment 28
LER: 9.276
SBD: 1.758
MD: 2.448
P: 28.195
CR: 1.631

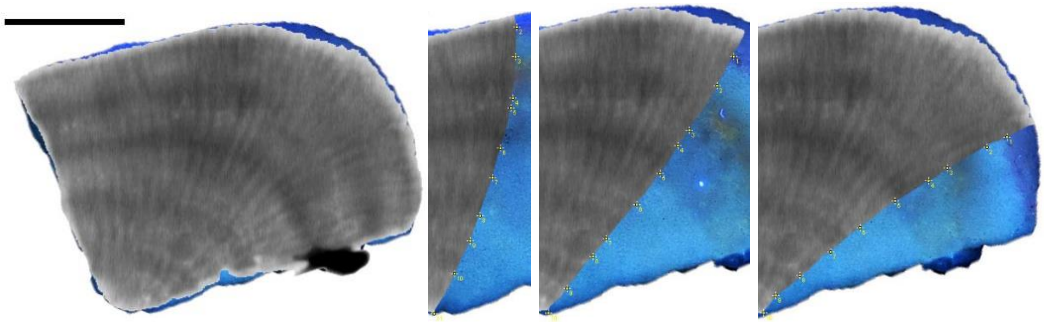

Fragment 29
LER: 10.935
SBD: 1.495
MD: 2.569
P: 41.792
CR: 1.635

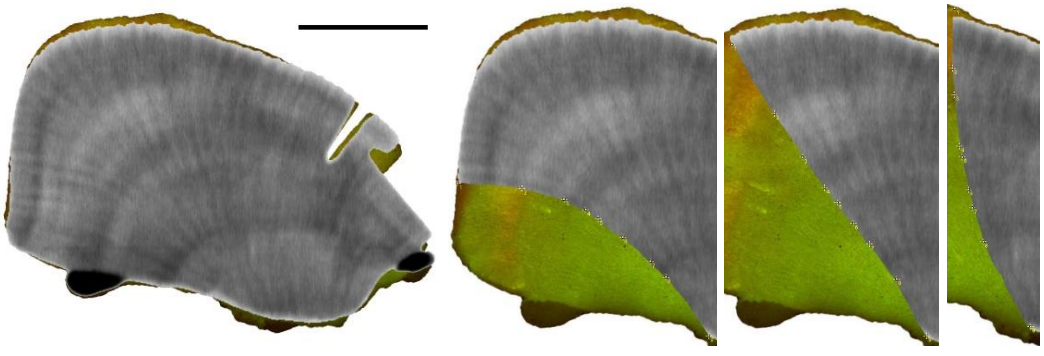

Fragment 30
LER: 8.533
SBD: 1.459
MD: 2.255
P: 35.317
CR: 1.245

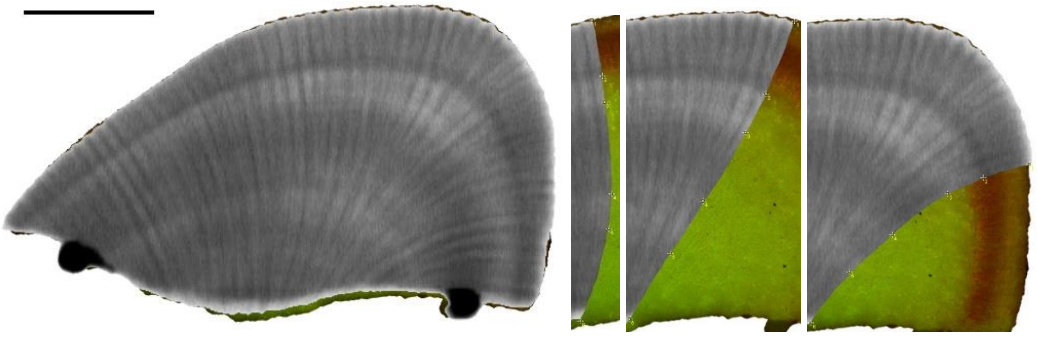

Fragment 32
LER: 8.603
SBD: 1.593
MD: 2.448
P: 34.946
CR: 1.370

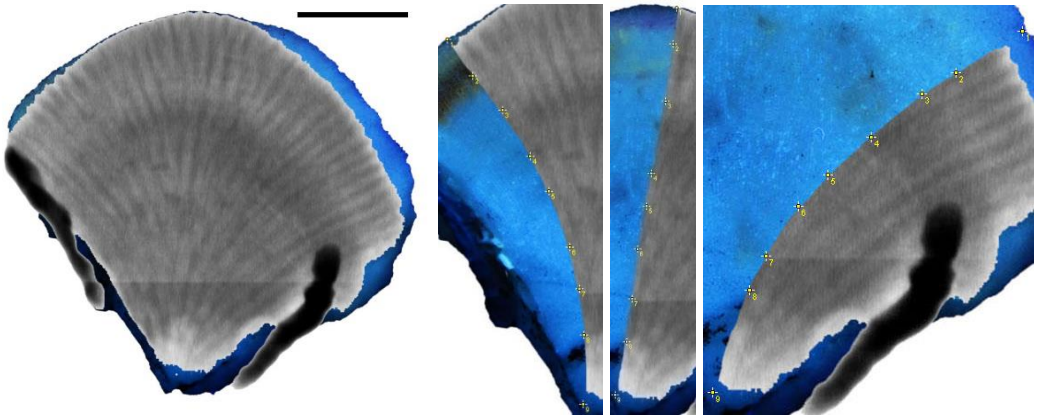

Fragment 33a
LER: 7.105
SBD: 1.516
MD: 2.128
P: 28.733
CR: 1.077

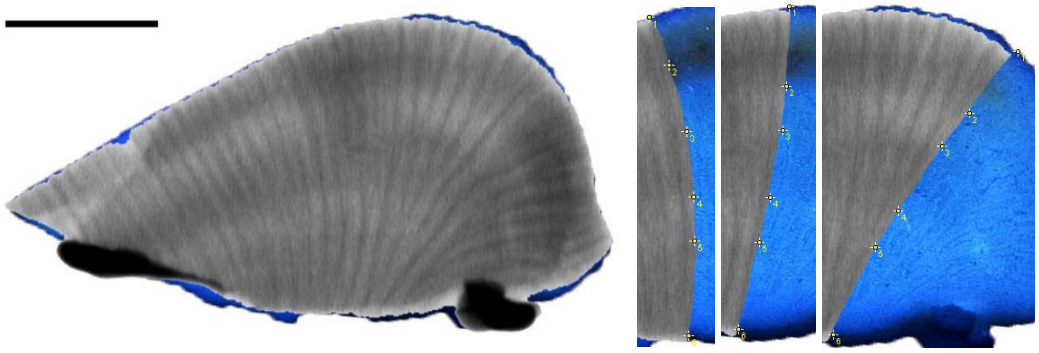

Fragment 33b
LER: 7.092
SBD: 1.576
MD: 2.345
P: 32.810
CR: 1.118

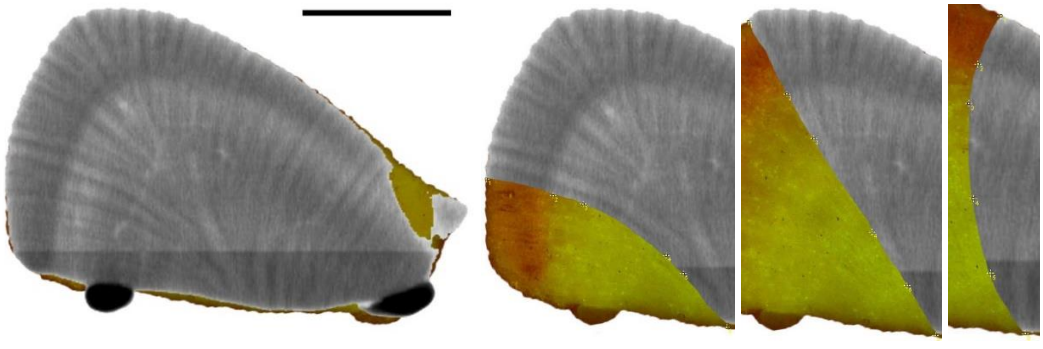

Fragment 34
LER: 8.511
SBD: 1.552
MD: 2.325
P: 33.240
CR: 1.321

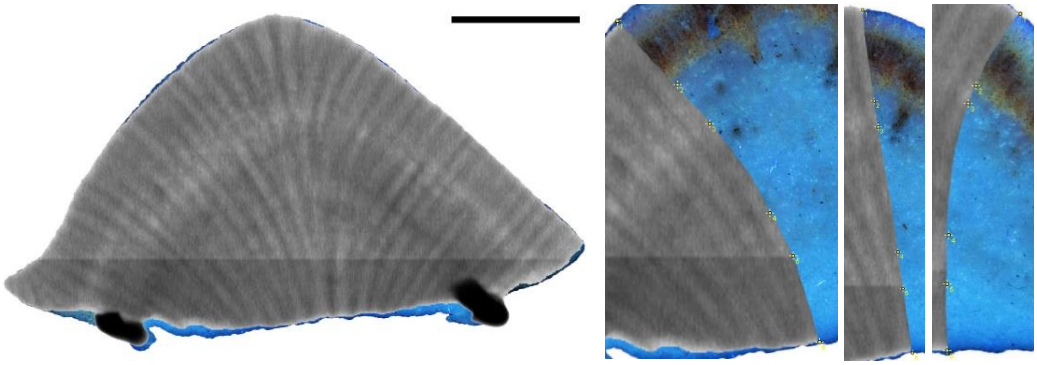

Fragment 37
LER: 9.331
SBD: 1.406
MD: 2.175
P: 35.344
CR: 1.312

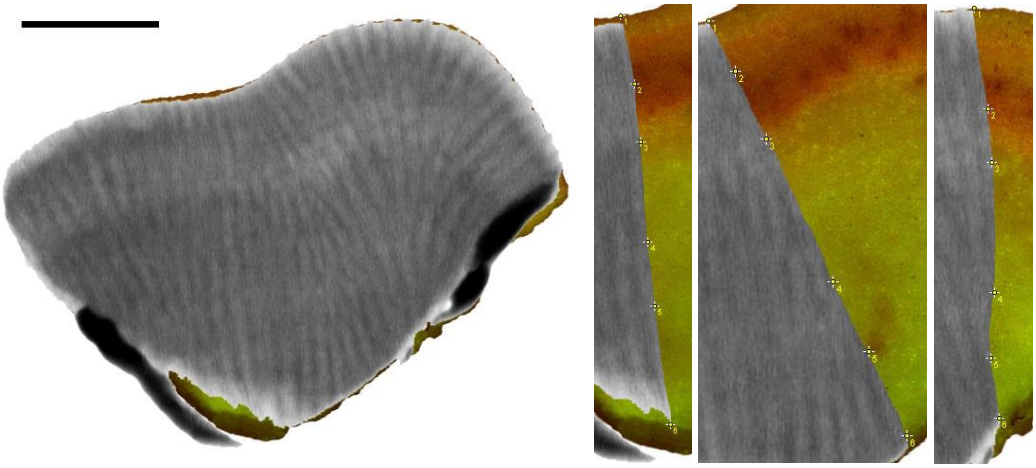

Fragment 38
LER: 10.159
SBD: 1.394
MD: 2.161
P: 35.479
CR: 1.417

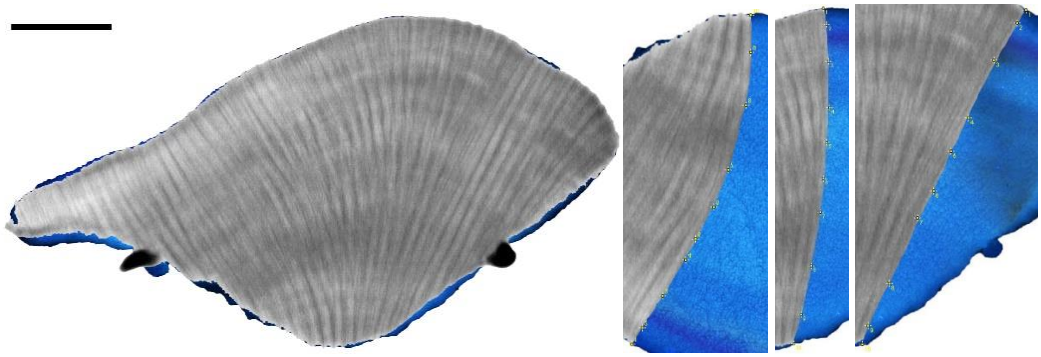

Fragment 39
LER: 7.853
SBD: 1.312
MD: 2.711
P: 51.610
CR: 1.030

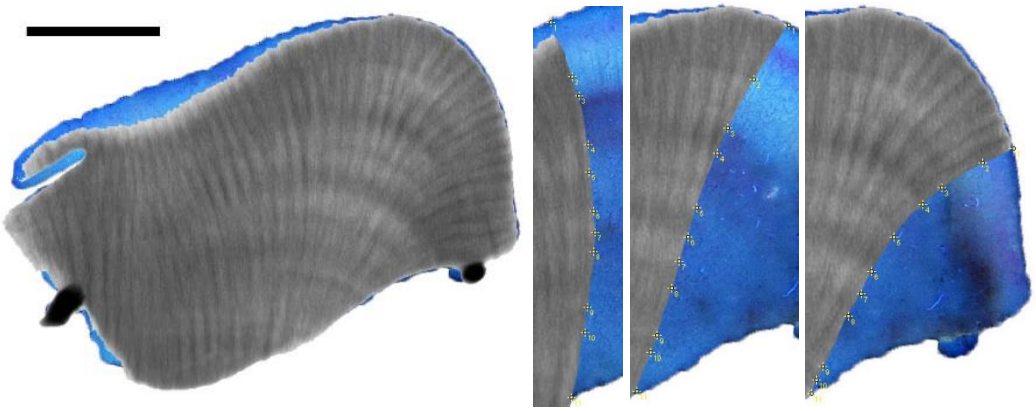

Fragment 40
LER: 8.150
SBD: 1.395
MD: 2.825
P: 50.622
CR: 1.137

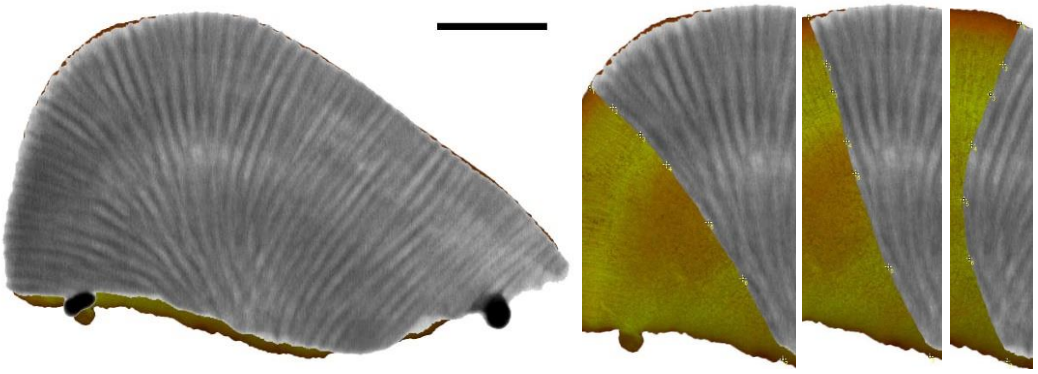

Fragment 41
LER: 8.807
SBD: 1.466
MD: 2.754
P: 46.760
CR: 1.291

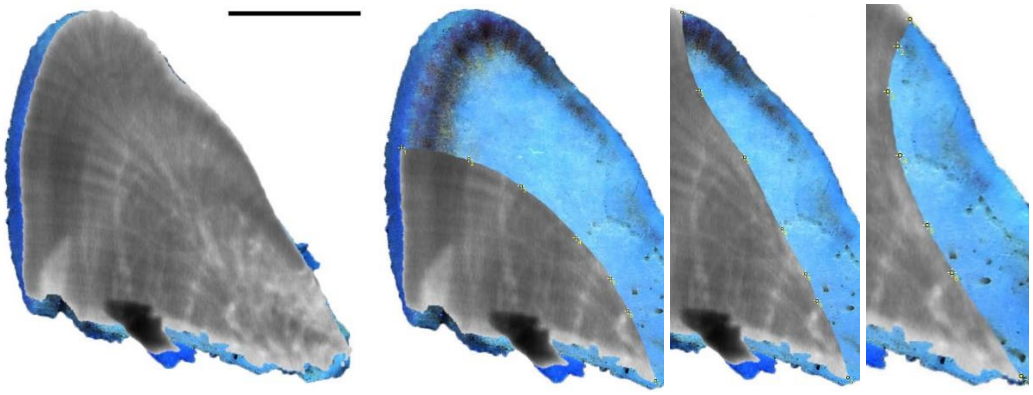

Fragment 43
LER: 7.786
SBD: 1.415
MD: 2.732
P: 48.197
CR: 1.102

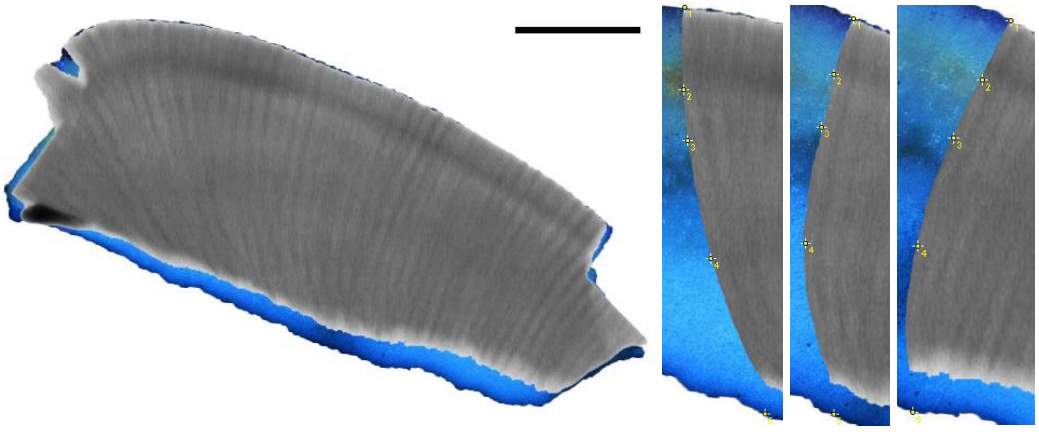

Fragment 44
LER: 9.332
SBD: 1.584
MD: 2.419
P: 34.505
CR: 1.479

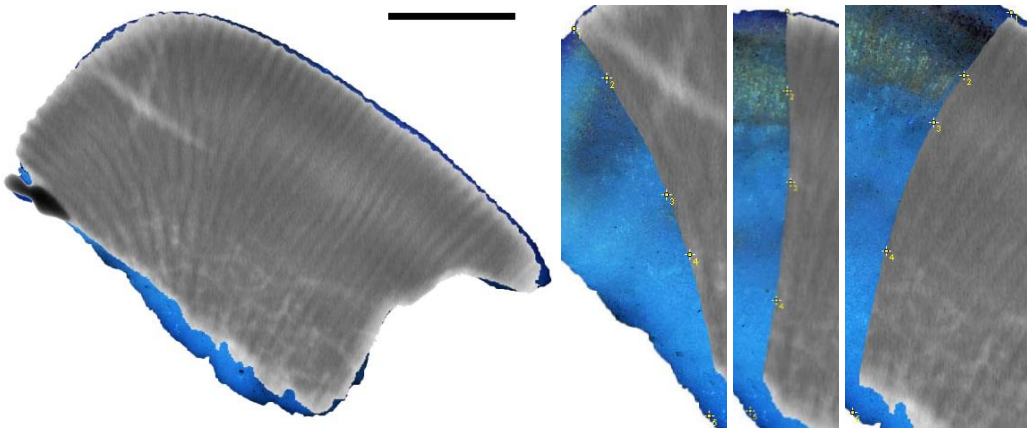

Fragment 45
LER: 11.474
SBD: 1.660
MD: 2.713
P: 38.804
CR: 1.905

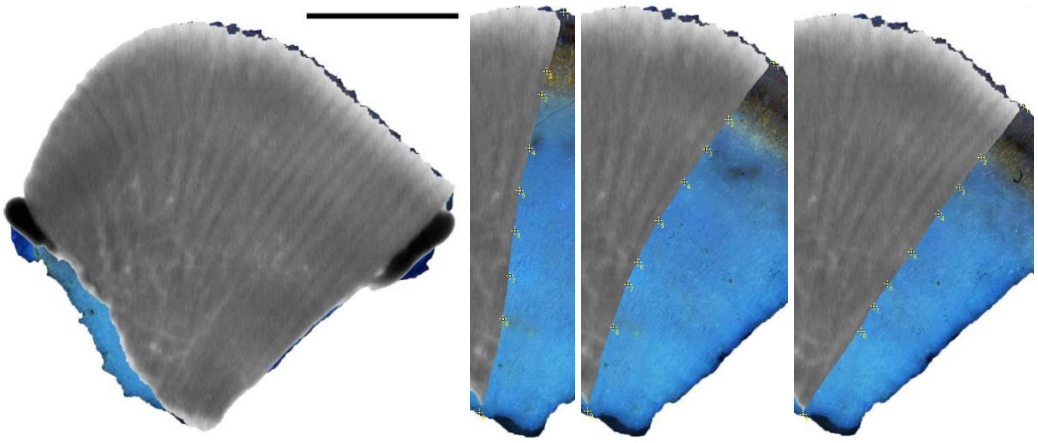

Fragment 46
LER: 9.548
SBD: 1.651
MD: 2.831
P: 41.669
CR: 1.577

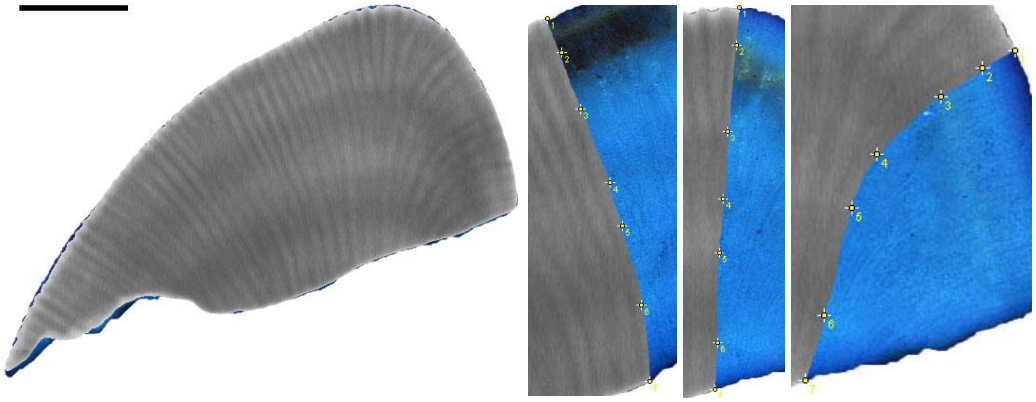

Fragment 47
LER: 7.988
SBD: 1.517
MD: 2.318
P: 34.562
CR: 1.212

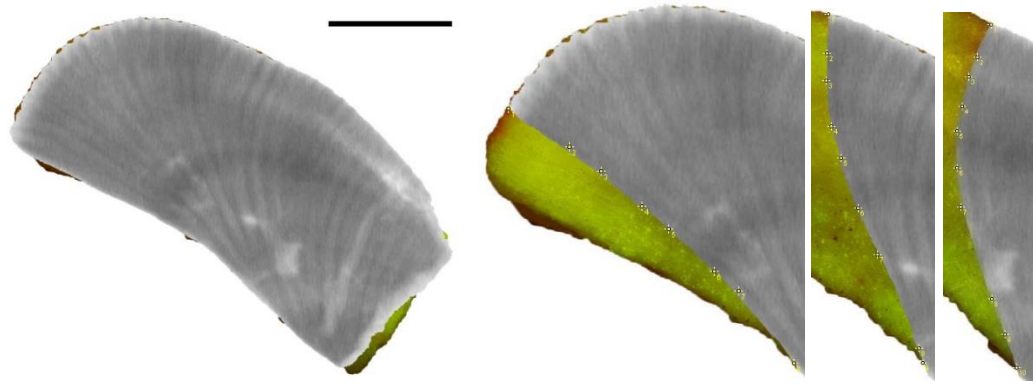

Fragment 48
LER: 9.263
SBD: 1.617
MD: 2.425
P: 33.306
CR: 1.498

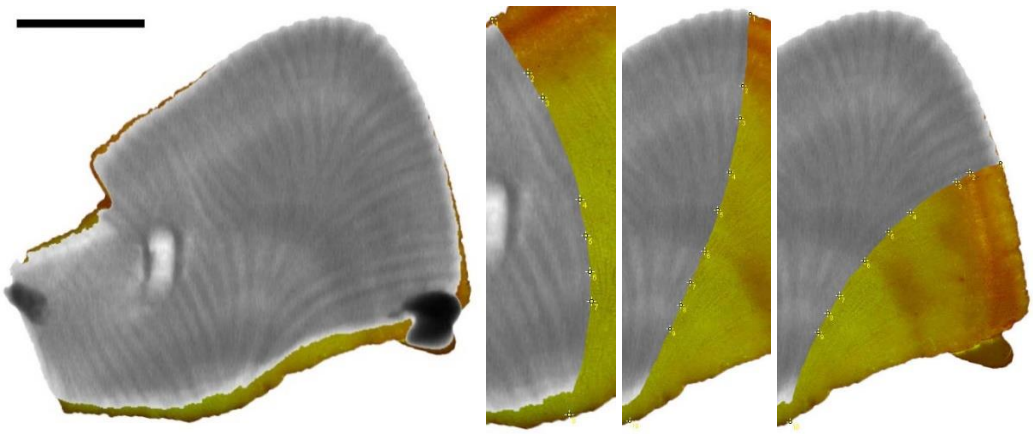

Fragment 49
LER: 9.662
SBD: 1.539
MD: 2.206
P: 30.218
CR: 1.487

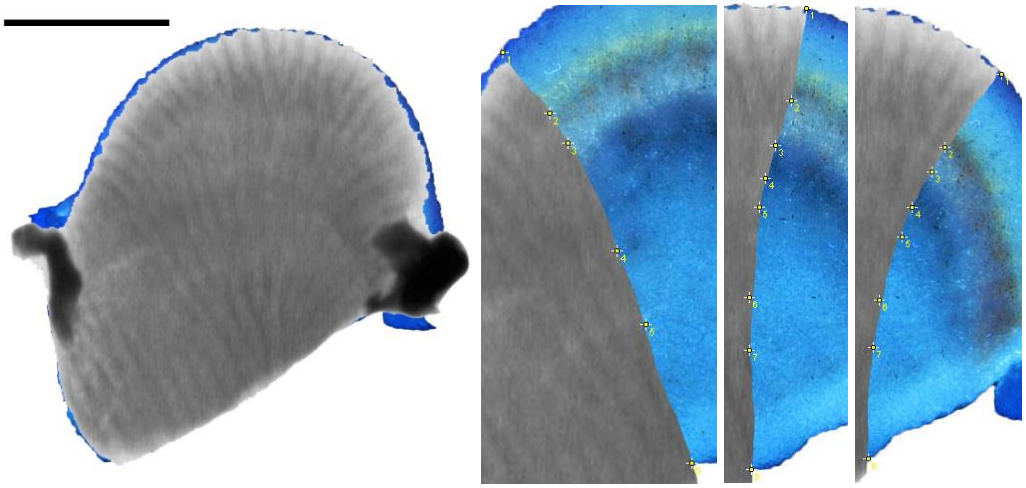

Fragment 50
LER: 7.434
SBD: 1.671
MD: 2.454
P: 31.885
CR: 1.243

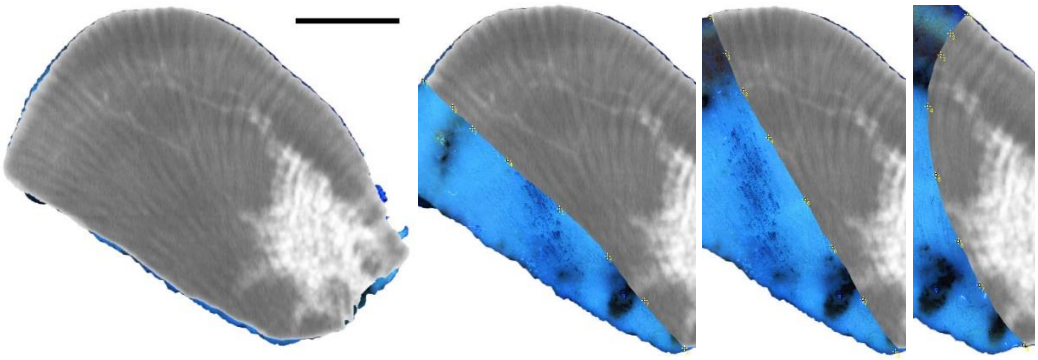

Fragment 51
LER: 9.824
SBD: 1.755
MD: 2.328
P: 24.608
CR: 1.724

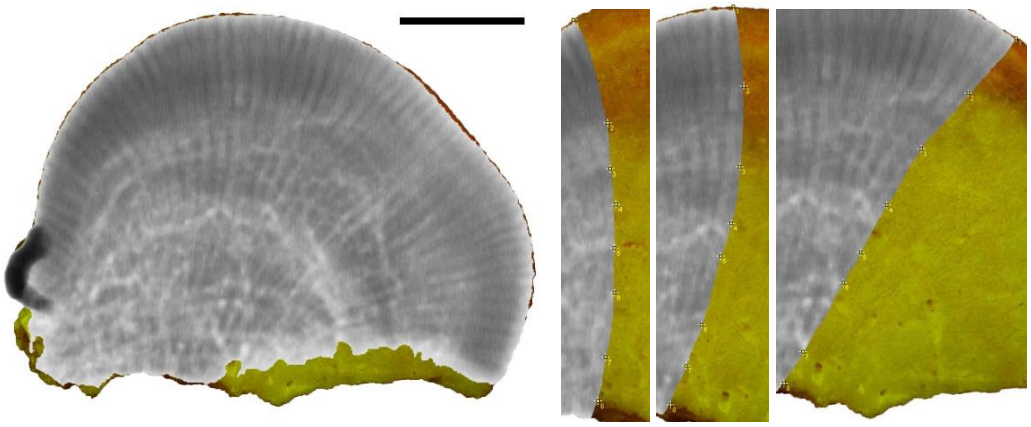

Fragment 52
LER: 7.532
SBD: 1.508
MD: 2.808
P: 46.294
CR: 1.136

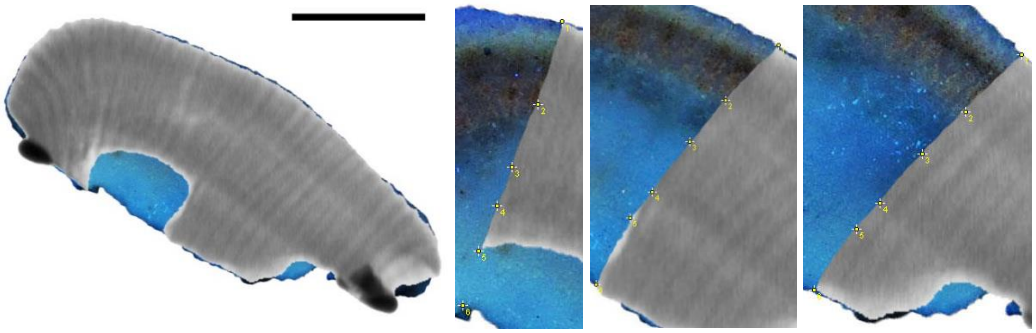

Fragment 53
LER: 9.125
SBD: 1.566
MD: 2.477
P: 36.789
CR: 1.429

Eigenständigkeitserklärung

Hiermit erkläre ich, dass die vorliegende Bachelorarbeit von mir selbstständig und ohne fremde Hilfe verfasst wurde. Es wurden nur die angegebenen Hilfsmittel und die im Literaturverzeichnis angegebenen Quellen verwendet und Zitate entsprechend im Text gekennzeichnet.

_____ _____

Ort, Datum Unterschrift